

# Optimizing Heat Alert Issuance with Reinforcement Learning

**Ellen M. Considine<sup>1</sup>, Rachel C. Nethery<sup>1</sup>, Gregory A. Wollenius<sup>2</sup>,  
Francesca Dominici<sup>1</sup>, Mauricio Tec<sup>1</sup>**

<sup>1</sup>Department of Biostatistics, Harvard T.H. Chan School of Public Health

<sup>2</sup>Department of Environmental Health, Boston University School of Public Health  
ellen\_considine@g.harvard.edu, mauriciogtec@hsph.harvard.edu

## Abstract

A key strategy in societal adaptation to climate change is using alert systems to prompt preventative action and reduce the adverse health impacts of extreme heat events. This paper implements and evaluates reinforcement learning (RL) as a tool to optimize the effectiveness of such systems. Our contributions are threefold. First, we introduce a new publicly available RL environment enabling the evaluation of the effectiveness of heat alert policies to reduce heat-related hospitalizations. The rewards model is trained from a comprehensive dataset of historical weather, Medicare health records, and socioeconomic/geographic features. We use scalable Bayesian techniques tailored to the low-signal effects and spatial heterogeneity present in the data. The transition model uses real historical weather patterns enriched by a data augmentation mechanism based on climate region similarity. Second, we use this environment to evaluate standard RL algorithms in the context of heat alert issuance. Our analysis shows that policy constraints are needed to improve RL's initially poor performance. Third, a post-hoc contrastive analysis provides insight into scenarios where our modified heat alert-RL policies yield significant gains/losses over the current National Weather Service alert policy in the United States.

### Code —

[https://github.com/NSAPH-Projects/heat-alerts\\_RL](https://github.com/NSAPH-Projects/heat-alerts_RL)

### Simulator —

<https://github.com/NSAPH-Projects/weather2alert>

### Extended version (with appendices) —

<https://arxiv.org/abs/2312.14196>

## 1 Introduction

Extensive evidence links exposure to extreme heat to increases in morbidity and mortality (Ebi et al. 2021). Heat alerts are a practical and low-cost intervention to mitigate these effects (Ebi et al. 2004) by encouraging protective measures such as hydrating more, avoiding physical exertion outdoors, and opening cooling centers. However, studies investigating the effectiveness of heat alerts have observed mixed results (Weinberger et al. 2018; Wu et al. 2023). Developing methods to optimize the issuance of heat alerts for public health is an open problem.

Copyright © 2025, Association for the Advancement of Artificial Intelligence ([www.aaai.org](http://www.aaai.org)). All rights reserved.

Various challenges stand in the way of solving this problem. First, issuing too many heat alerts may lead to alert fatigue (Nahum-Shani et al. 2017) and health-protective resource depletion on both individual and community/institutional levels. Sequential decision-making (SDM) methods offer a promising yet unexplored avenue for tackling this issue. Second, despite representing a significant health threat on the population scale, local health impacts of heat—and therefore heat alerts—are small and easily confounded in observational data sets (Weinberger et al. 2021). Rare events and low signal (small effects) have been shown to challenge algorithmic decision-making (Frank, Mannor, and Precup 2008; Romoff et al. 2018). Third, mainstream SDM methods are not suitable for spatially heterogeneous settings in which a single policy is not equally effective in all regions or dynamically changing contexts (Padakandla 2021). However, attempting to identify independent policies for each location drastically reduces the amount of available historical data.

In this paper, we lay the foundation for addressing these challenges by introducing a framework for optimizing heat alert issuance using reinforcement learning (RL). RL allows learning SDM policies for determining when to issue heat alerts, aiming to minimize the population health risk as a negative reward signal. The ultimate vision for this vein of research is deploying data-driven policies to alert the public about extreme heat events (and, eventually, other environmental exposures such as extreme cold or wildfire smoke). In addition to our analysis breaking ground towards this goal, a variety of follow-up work is facilitated by the publication of our SDM environment in an open-source Python package, `weather2alert`<sup>1</sup>, compatible with the Gymnasium framework for RL (Towers et al. 2023). This challenging, data-driven environment can be used as a benchmark. Further, our methodology to create this environment can be used as a blueprint for other RL simulators, particularly for problems with exogenous state space components and multiple locations or individuals.

The two main components of our heat alerts RL framework are visualized in Figure 1 and summarized below. First, we create a realistically challenging SDM environment for heat alert issuance, structured as a Markov Decision Process (MDP) under a budget constraint. Key compo-

<sup>1</sup><https://github.com/NSAPH-Projects/weather2alert>

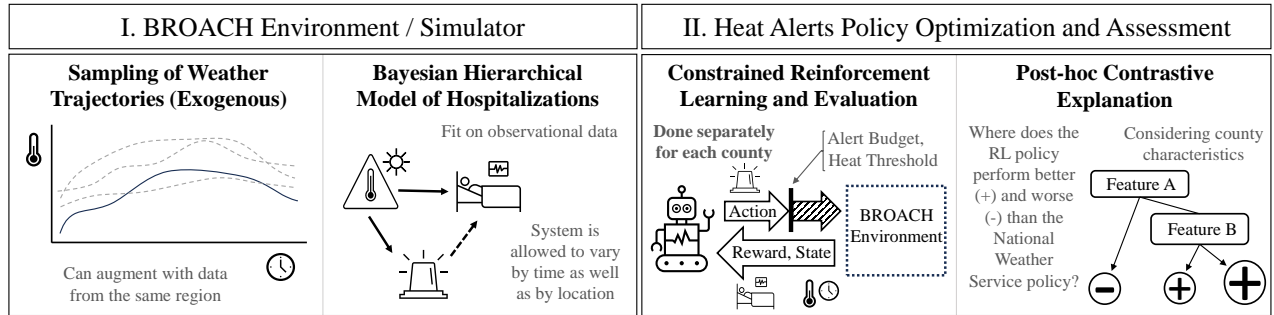


Figure 1: Overview of the heat alerts RL framework.

ments of the dataset used to create this environment are heat alerts issued by the U.S. National Weather Service (NWS), hospitalization records from Medicare, ambient heat index, and other covariates informed by the epidemiological literature. To estimate the rewards under both observed (NWS) and counterfactual alert policies, we fit a statistical model of hospitalizations that allows for spatiotemporal heterogeneity, uncertainty quantification, and fast inference using variational Bayes (Tzikas, Likas, and Galatsanos 2008). For the state-transition model, we exploit a factorization of the state space into an endogenous component with known transition dynamics and an exogenous component sourced from observed weather trajectories. This use of real data allows us to make grounded inferences about the effectiveness of both observed and counterfactual heat alert policies in the U.S. We call this environment structure Bayesian Rewards Over Actual Climate History (BROACH).

Second, we use our environment to train RL models and then to evaluate the RL policies as well as the NWS and alternative baseline policies—all subject to the same alert budget. Our evaluation identifies issues during training that lead to poor performance of standard, widely-used RL algorithms. We address these issues by introducing conceptually simple modifications which enable learning of policies that reduce hospitalizations relative to the NWS policy. These modifications include restricting the RL model to issue alerts only on extremely hot days and optimizing policies for each location separately. Lastly, we perform contrastive explanation (van der Waa et al. 2018; Narayanan, Lage, and Doshi-Velez 2022) of the RL policies by comparing their attributes (e.g., how often does the policy issue alerts on consecutive days) within and across locations to those of the NWS and alternative baseline policies. Specifically, we use visualizations and Classification and Regression Trees (CART) to illustrate systematic differences between these policies and identify characteristics of locations where RL-based policies might offer the greatest improvements in public health.

## 2 Related work

**Heat alert optimization** Recent approaches to improving the issuance of heat alerts include (i) the development of a causal inference technique for stochastic interventions to infer whether increasing the probability of issuing a heat alert would be beneficial (Wu et al. 2023) and (ii) a comparison

of methods to identify optimal thresholds above which heat alerts should always be issued (Masselot et al. 2021). Crucially, neither of these approaches addresses the complications of sequential dependence, i.e., the potential for alert fatigue and running out of resources to deploy precautionary measures. To our knowledge, SDM techniques have not yet been explored in a climate and health setting.

**RL with exogenous states** Several recent papers utilize a decomposition of the state space into exogenous vs. endogenous components, but none of these methods apply directly in our setting. Efroni et al. (2022) provide theoretical analysis and guarantees for sample efficiency in tabular (finite state) environments with an unknown subset of exogenous variables. Sinclair et al. (2023) introduce “hindsight learning” for situations with a known reward function and an exact solver under a fixed exogenous trajectory. Lee et al. (2023) also use hindsight, but do so in the context of identifying latent states within a partially observable MDP. Contrary to Levine, Stone, and Zhang (2024) and Efroni et al. (2024), we do not consider exogenous states as distractors since weather patterns are crucial for decision-making.

**Statistical modeling for RL environments** Using a statistical model for the reward function in an RL environment is common practice in settings with empirical data. Bayesian models in particular have been used to identify the effect of intervention in health-related applications and dynamic treatment regimes (Liao et al. 2020; Tec, Duan, and Müller 2023; Zajonc 2012). For spatiotemporal or otherwise heterogeneous environments, previous studies have also used a combination of local modeling and global modeling that takes into account the spatial or hierarchical structure to create simulated environments for RL (Wu et al. 2021; Li, Zheng, and Yang 2018; Agarwal et al. 2021).

**Constrained learning** The use of domain knowledge-based policy restrictions in RL has been found to speed up learning and to guide the learned policy in pragmatic directions (Mu et al. 2021). This supports our restriction of RL heat alerts to very hot days. More generally, incorporating “cost” or “safety” constraints is of interest for many RL applications (Laber et al. 2018; Carrara et al. 2019). A common approach in the constrained RL literature is to use Lagrange multipliers (Guin and Bhatnagar 2023; Ray, Achiam, and Amodei 2019), however, these methods do not enforce

a strict constraint/budget. To enable direct comparison with the observed NWS policy, we impose a strict alert budget, which can be viewed as a simplified variation of the indicator approach formulated by Xu, Zhan, and Zhu (2022). An alternative approach to handling both the alert budget and restriction of alerts to very hot days would be to model the extent of distributional overlap with the observed NWS policy, and penalize actions that have too little overlap (Xu, Zhan, and Zhu 2022). However, our approach has the benefit of being relatively interpretable.

**Contrastive policy explanations** There is a large literature on post-hoc explainability in RL (Heuillet, Couthouis, and Díaz-Rodríguez 2021). Contrastive analysis has been used to explain differences between RL policies and more familiar / intuitive policies (van der Waa et al. 2018; Narayanan, Lage, and Doshi-Velez 2022). We note that while CART has been used to try and mimic RL policies (Puiutta and Veith 2020), our use of it to analyze differences between policies has not been previously documented.

### 3 Problem Setup

#### 3.1 RL Preliminaries

RL methods typically operate within the framework of Markov Decision Processes or MDPs (Sutton and Barto 2018). A finite-horizon or episodic MDP with horizon (episode length)  $H$  is defined as a tuple  $\mathcal{M} = \langle S, A, R, P, d_0, \gamma \rangle$ , where  $S$  is the set of states,  $A$  is the set of actions,  $R : S \times A \rightarrow \mathbb{R}$  is the expected reward function,  $P : S \times A \rightarrow \Delta(S)$  is the transition function<sup>2</sup>,  $d_0 \in \Delta(S)$  is the initial state distribution, and  $0 < \gamma \leq 1$  is the time discount factor<sup>3</sup>. A (non-stationary) policy is defined as a collection of decision rules  $\pi = \{\pi_t : S \rightarrow \Delta(A)\}_{t=0}^{H-1}$ , mapping from states to probability distributions over actions at each time step. The state value function is  $V_t^\pi(s) := \mathbb{E}_\pi [\sum_{h=t}^{H-1} \gamma^{h-t} R(s_h, a_h) | s_t = s]$  and the state-action value function is  $Q_t^\pi(s, a) := R(s, a) + \gamma \mathbb{E}_{s' \sim P(s, a)} [V_t^\pi(s')]$ . The policy optimization goal is to identify  $\pi^*$  that maximizes the expected cumulative reward

$$J(\pi) := \mathbb{E}_{s_0 \sim d_0} [V_0^\pi(s_0)]. \quad (1)$$

Under regularity conditions (Puterman 2014), the optimal policy is deterministic and the unique solution (up to ties) of the Bellman optimality equation

$$Q_t^*(s, a) = R(s, a) + \gamma \mathbb{E}_{s' \sim P(s, a)} [\max_{a'} Q_{t+1}^*(s', a')], \quad (2)$$

where  $Q_t^*$  denotes the state-action value function of  $\pi_t^*$ . The optimal action satisfies  $\pi_t^*(s) = \arg \max_a Q_t^*(s, a)$ .

RL algorithms search for the optimal policy of an MDP by interacting with an environment that generates rewards and transitions, where the RL algorithm does not need knowledge of the transition function (Sutton and Barto 2018).

<sup>2</sup> $\Delta(\cdot)$  is the set of probability distributions over the set “.”.

<sup>3</sup>Note that in our analysis,  $\gamma = 1$  works best, so in practice there is no discounting.

#### 3.2 Issuing Heat Alerts as a Constrained MDP

The heat alerts MDP components are summarized here. See also Table S1 of Appendix A. Each MDP  $\mathcal{M}_k$  corresponds to a geographic area  $k \in \mathcal{K}$ , and episodes are indexed as  $j \in \mathcal{J}$ . In this work, geographic areas are U.S. counties, and each episode spans the warm season / summer from May 1st to September 30th of a specific year ( $H = 152$  days).

The action  $a_t$  on day  $t$  is either 1 (issue a heat alert) or 0 (do not issue a heat alert). To mitigate alert fatigue, we adopt a strict action budget-constrained approach, optimizing the policy subject to  $\sum_{t=0}^{H-1} a_t \leq b$ .

The reward  $r_t = R(s_t, a_t)$  is the expected rate of heat-related hospitalizations at time  $t$ , transformed such that fewer hospitalizations correspond to a greater reward. Specifically, if  $\rho_t(a_t) := \rho(s_t, a_t)$  represents the *per capita* rate of heat-related hospitalizations on day  $t$  if action  $a_t \in \{0, 1\}$  is taken at state  $s_t$ , then  $r_t \propto -\rho_t(a_t) + \text{const}$ .

The state vector  $s_t$  contains the factors underlying the effect of heat on hospitalizations and the effectiveness of heat alerts at reducing hospitalizations. It can be decomposed as  $s_t = (\xi_t, x_t)$ , where  $\xi_t$  is the exogenous component and  $x_t$  is the endogenous component. The exogenous component is defined as the portion of the state space that is not influenced by the agent’s actions  $a_t$ , such as the weather. The transition function of the endogenous component (heat alert history) is known and deterministic. Hence, the full state transition function admits a factorization

$$\begin{aligned} P(s_{t+1} | s_t, a_t) &= P((\xi_{t+1}, x_{t+1}) | (\xi_t, x_t), a_t) \\ &= P_\xi(\xi_{t+1} | \xi_t) P_x(x_{t+1} | x_t, a_t) \end{aligned} \quad (3)$$

### 4 BROACH: An RL Environment for Optimizing Heat Alert Issuance

In creating an interactive heat alert environment, our design objectives are (i) allow use of general-purpose RL algorithms, (ii) be grounded in real data, and (iii) handle the low signal and heterogeneity of health impacts of heat and heat alerts across space and time. To meet these objectives, we introduce a methodology termed Bayesian Rewards Over Actual Climate History (BROACH). BROACH can be generalized to other climate-related events and interventions.

#### 4.1 Data Sources

Here we provide an overview of the data used in the RL environment; Appendix B contains more details.

**Heat alerts and heat index** We use the dataset of Weinberger et al. (2021) with daily, county-level records (2006-2016, May-September) of heat alerts issued by the NWS, as well as heat index, which is a measure of the combined effect of temperature and humidity. To understand the observed heat alert data, note that while the decision to issue an alert is based on temperature thresholds, it is also strongly affected by the discretion of the local office (Hawkins, Brown, and Ferrell 2017). Analysis by (Hondula et al. 2022) suggests that spatial variability in the current NWS/local office approach is not well aligned with the health risk from heat.

**Heat-related hospitalizations** We merged the heat alert and weather data with daily, county-level hospitalization counts from Medicare. We included cause-specific hospitalizations previously found to be associated with extreme heat in the Medicare population: septicemia, peripheral vascular disease, urinary tract infections, and diabetes mellitus with complications (Bobb et al. 2014). We excluded heat stroke and fluid and electrolyte disorders (which were also found to be associated with extreme heat in Medicare) because Weinberger et al. (2021) observed a positive association between heat alerts and hospitalizations with these causes. They hypothesized it was due to increased awareness of heat-related symptoms and seeking medical care. Figure S1 illustrates this scenario as an unobserved mediation problem (Pearl 2012), which affects the identification of the preventive effect of heat alerts. We refer to the remaining causes, which we pool together into one outcome variable, as not-obviously heat-related (NOHR) hospitalizations.

**Counties** We consider the 761 counties with a population greater than 65,000 to avoid locations with very few hospitalizations and to focus on the most populous areas. Figure 2 shows the counties considered, which account for approximately 75% of the population and 25% of the number of counties.

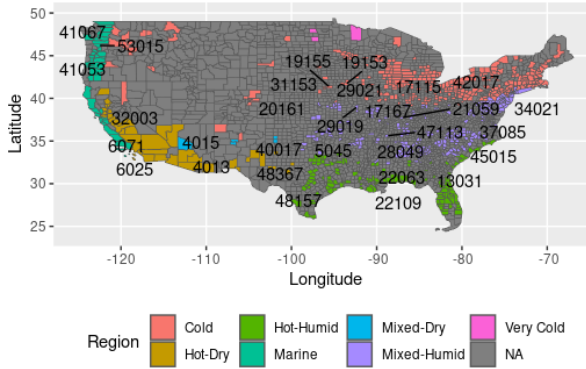


Figure 2: Map of the counties considered and their regional climate zone classifications. All the colored counties are used in the Bayesian rewards model and RL environment; the 30 counties with annotated FIPS codes are used in the RL experiments.

**County-level characteristics** Spatial heterogeneity in the health effects of heat and heat alerts can occur due to people in different regions being affected differently by the same absolute temperatures due to geographical self-selection and climate adaptation, differential health susceptibility and/or individual agency associated with socioeconomic status and population density, and variable response to heat alerts due to local policy and political ideology (Ng et al. 2014; Zanobetti et al. 2013; Errett et al. 2023; Cutler et al. 2018). To characterize this spatial heterogeneity, we compiled a set of county-level covariates: population density and median household income (U.S. Census Bureau 2014), regional

classifications of climate zones (U.S. Energy Information Administration 2020), broadband (internet) usage data (Microsoft AI for Good Research Lab 2021), presidential election returns (MIT Election Data and Science Lab 2018), and fine particulate matter ( $PM_{2.5}$ ) (Hammer et al. 2020). For the latter, there is strong evidence of adverse synergistic health impacts of air pollution and heat (Anenberg et al. 2020).

## 4.2 The State Space

Recall that the state space can be factorized as  $s_t = (\xi_t, x_t)$ , where  $\xi_t$  is the exogenous component and  $x_t$  is the endogenous component. The exogenous component contains the quantile value of the day’s observed heat index (QHI)—within each county across warm seasons for all the years—which allows us to account for long-term climate adaptation. It also contains time-varying factors which can modify the heat-health relationship (Heo, Bell, and Lee 2019; Anderson and Bell 2011): day of summer (which is equivalent to  $t$ ), weekend status, and excess heat compared to the last three days. The endogenous component contains the number of heat alerts issued in the last 14 days, an indicator of whether a heat alert was issued yesterday, and the remaining alert budget for that episode.

## 4.3 The Reward Function: A Hierarchical Model of Hospitalizations

To learn the expected hospitalization rate, and thereby the transformed reward  $r_t$ , we train a Bayesian hierarchical model with the desiderata of (a) facilitating obtainment of confidence intervals when evaluating RL policies and (b) allowing for spatial heterogeneity in the health effects of heat and heat alerts. Let  $\rho_t^{(k,j)}(a)$  be the expected per capita NOHR hospitalization rate at time  $t$  in county-summer  $(k,j)$  when taking action  $a$ . We propose the scaled reward function  $r_t^{(k,j)}(a) := C_1 - C_2 \rho_t^{(k,j)}(a)$  where  $C_1$  and  $C_2$  are positive scaling constants. (Note that choices of  $C_1$  and  $C_2$  do not change the optimal policy, but can help stabilize learning.) We choose  $C_1 = 1$  and  $C_2$  as the reciprocal of the observed hospitalization rate through the entire summer.

Let  $y_t^{(k,j)}(a)$  denote the counterfactual outcome representing the number of NOHR hospitalizations for action  $a \in \{0, 1\}$ , and  $n^{(k,j)}$  denote the total population susceptible to hospitalization in county  $k$  in episode  $j$ . We introduce two functions—to be learned—governing the counterfactual hospitalization rate in county  $k$  as a function of  $s_t^{(k,j)}$ . First,  $\lambda_k: S \rightarrow \mathbb{R}^+$  denotes the baseline rate of hospitalizations when no alert is issued. Second,  $\tau_k: S \rightarrow (0, 1)$  expresses the effectiveness of issuing an alert as a multiplicative reduction factor. The top-level hospitalization model is

$$y_t^{(k,j)}(a) \sim \text{Poisson}(n^{(k,j)} \rho_t^{(k,j)}(a)), \quad (4)$$

$$\rho_t^{(k,j)}(a) := \lambda_k(s_t^{(k,j)})(1 - a \cdot \tau_k(s_t^{(k,j)})),$$

for all  $(k, j) \in \mathcal{K} \times \mathcal{J}$  and  $t \in \{0, \dots, H-1\}$ . The Poisson distribution/loss function is the natural choice for count data and recommended for health outcomes data due to its correspondence to the Cox survival model (Austin 2017).

To estimate the functions  $\lambda_k$  and  $\tau_k$  under limited data and low health signal, we incorporate a data-driven random effects prior (using the county-level features) and inject domain knowledge on the signs of certain coefficients. We train this model using variational inference, using the Python package Pyro (Harpole et al. 2019). **The details of this approach, as well as model diagnostics, are in Appendix C.** Note that the fitted coefficients in the alert effectiveness component indicate the presence of alert fatigue. To utilize this rewards model within the BROACH environment, we draw from the variational posterior distribution at the start of each episode, and then use those coefficients to calculate  $r_t^{(k,j)}$  given  $(s_t^{(k,j)}, a_t^{(k,j)})$  for  $t = 0, \dots, H - 1$ .

#### 4.4 The Alert Budget

Each episode in our MDP starts with a fixed alert budget  $b$ . This can be specified as a constant, sampled from a range of values, or set to the observed (NWS) value. As the agent steps through the episode, once  $\sum_{h=0}^t a_h = b$ , it is prohibited from issuing any more alerts: it can only obtain the reward  $r_h^{(k,j)}(0)$  for days  $h = t + 1, \dots, H - 1$ .

#### 4.5 The Transition Function: Observing Actual Weather/Climate History

We leverage the decomposition equation 3 to use real data for the exogenous trajectories, and introduce a data augmentation scheme in the context of single-county RL.

**Sampling of exogenous trajectories** Recall that the endogenous aspect of our state space, heat alert history, is deterministically updating, so does not need to be modeled probabilistically. The key observation in the heat alert setting is that the more complicated aspect of the environment, the weather/climate, also does not need to be modeled because it is completely exogenous to heat alert decision-making. In this setting, developing a model for the weather is not only unnecessary, but would unavoidably introduce error. Instead, we sample real observed weather trajectories.

**Regional data augmentation** The issue with this approach is that there are only 11 years of exogenous trajectories (2006-2016) available per county during which we also have heat alert data—which is needed when we use observed alert budgets (paired with observed weather) for comparison with the NWS. To mitigate the potential for RL overfitting to these 11 years, we propose data augmentation by sampling exogenous trajectories from other counties in the same regional climate zone<sup>4</sup> (U.S. Energy Information Administration 2020) during RL training and validation / tuning.

### 5 Learning and Evaluation

We conduct experiments to (a) assess the ability of standard RL algorithms to learn effective heat alert policies in the BROACH environment, (b) test various modifications to these algorithms, and (c) compare the resulting policies to

<sup>4</sup>Due to the large size/geographic range of the “Cold” zone, we grouped its counties into eastern and western subsets.

the NWS policy and other intuitive baselines. We then investigate heterogeneous performance of the RL policies to provide domain-relevant insights. Code for all steps is available in our GitHub repository<sup>5</sup>.

#### 5.1 Policy Constraint: Very Hot Days

Foreshadowing our findings, standard RL algorithms struggle to learn to conserve their alert budgets for later in the summer, resulting in poor performance. A major modification we implement to encourage more effective behavior is restricting the issuance of heat alerts to days above a QHI threshold, optimized separately for each county. To optimize the QHI threshold, we test the sequence of values between 0.5 and 0.9 (ensuring overlap with the NWS policy), by every 0.05, and select the value that yields the best return on our validation set (specified in the following section). Names of models including this adaptation have the suffix “.QHI”.

#### 5.2 Experimental Setup

For all training and evaluations, to directly compare counterfactual alert policies with the NWS policy, we fix  $b$  in each county-summer to the observed number of heat alerts.

**RL baselines** We investigate using four common RL algorithms: Deep Q-learning (DQN), Quantile Regression Deep Q-learning (QRDQN), Trust Region Policy Optimization (TRPO), and Advantage Actor-Critic (A2C)—additional information on these algorithms is in Appendix D.2. We use standard implementations of these methods available in the `Stable-Baselines3` Python library (Raffin et al. 2021). To ground our analysis and discussion, note that DQN and QRDQN are off-policy methods which learn deterministic policies by directly solving for the optimal value function using the Bellman optimality condition in equation 2; exploration is induced only during training (e.g. epsilon-greedy). Whereas, TRPO and A2C are on-policy methods which learn stochastic policies by direct optimization of the expected return in equation 1, using refinements of the policy gradient theorem (Sutton et al. 1999); exploration is inherent.

**NWS and simple alternative baselines** To evaluate each of the RL policies, we compare them to the observed NWS policy as well as several counterfactual baselines: most simplistically, randomly selecting  $b$  days on which to issue alerts (RANDOM) and selecting the  $b$  days with the highest QHI that summer (TOPK)—the latter is an oracle policy (not implementable in the real world) because to use it, we would have to know the whole summer’s daily QHI in advance. We also implement the general guidelines that NWS recommends in the absence of local criteria for issuing heat alerts (BASIC.NWS): alert if the heat index is  $\geq 100^{\circ}\text{F}$  in northern states and  $\geq 105^{\circ}\text{F}$  in southern states (Hawkins, Brown, and Ferrell 2017). Lastly, we implement a policy of always issuing alerts on days above a per-county optimized QHI threshold until the budget runs out (AA.QHI).

<sup>5</sup><https://github.com/NSAPH-Projects/heat-alerts.RL>

**Training data** The counties for which NWS issued few heat alerts had high-variance estimates of heat alert effectiveness in the rewards model. Therefore, for the RL experiments, we selected a subset of 30 counties in which at least 75 heat alerts were issued during 2006-2016; spread across the five major climate regions, prioritizing those with higher variance in estimated alert effectiveness across days. See map in Figure 2 and Appendix D.1 for more details.

**Evaluation metric** The main metric we use for policy comparison is the average cumulative reward per episode (“average return”). To estimate this metric fairly, we hold three years of data (2007, 2011, and 2015) out of RL training, referred to as the evaluation years<sup>6</sup>. For the purposes of RL hyperparameter tuning (details in Appendix D.3) and selection of the optimal QHI threshold for each county, we consider the regionally augmented weather trajectories and associated heat alert budgets from the evaluation years *excluding the county of interest* to be the validation data set. The final evaluation results (reported in tables and figures) are obtained by drawing 1,000 sets of coefficients from the Bayesian rewards model posterior and calculating the return under each policy with weather and budgets *only from the county of interest* during the evaluation years. These validation/tuning and evaluation procedures are described algorithmically in Appendix E. After calculating the average returns for the 30 counties under each competing policy, we compare each policy’s returns with the associated returns under the NWS policy using a Wilcoxon-Mann-Whitney test. This nonparametric test allows us to compare the distribution of differences in returns, accounting for the fact that the counties are highly heterogeneous, so the differences between the policies are not normally distributed.

**Sensitivity analysis** In the main analysis, we evaluate each county-specific implementation of DQN, QRDQN, TRPO, and A2C by allowing each algorithm to deploy the type of policy that it optimizes during training: deterministic for DQN and QRDQN and stochastic for TRPO and A2C. As a sensitivity analysis, we also deterministically evaluate the TRPO and A2C policies, selecting whichever action has a higher probability under the policy function. The names of these models have the prefix “DET”. In another sensitivity analysis, we investigate whether the RL models can learn to anticipate subseasonal variation in the warm season by augmenting the RL state space with information about the future. Specifically, we test whether inclusion of the change in heat index over each of the next 10 days, as well as the 50th-100th (by every 10) percentiles of QHI for the remainder of the summer, improves RL performance. In real-time deployments of RL models, this kind of future information would not be known but could be sourced from weather forecasts or climate model projections. Of course, such forecasts / model projections are not perfect, but we start with perfect future information as a proof of concept. The names of models that include future information have the suffix “.F”.

<sup>6</sup>Appendix D.4 shows the results of a sensitivity analysis where the models are trained on 2006-2013 and evaluated on 2014-2016.

### 5.3 Results and Discussion

Figures 3, S5, and S6 illustrate how the different policies look in practice, respectively in scenarios where using RL is beneficial, where the alert budget is small, and where using RL is not beneficial compared to the alternatives.

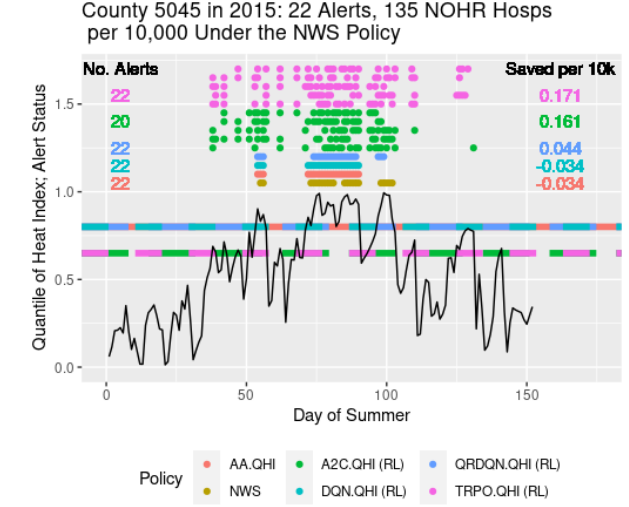


Figure 3: An example of observed and counterfactual heat alert policies for a single summer (2015 is the most recent year in our evaluation set), with estimates of the number of NOHR hospitalizations saved (compared to NWS) per 10,000 Medicare enrollees under each policy. The dashed lines indicate the optimized QHI threshold of the policy in the same color. The multiple horizontal lines of pink and green dots indicate five different samples from TRPO.QHI and A2C.QHI respectively. For these two policies, the number of NOHR hospitalizations saved is the average of all their evaluations over 2015.

Table 1 provides the main results of our RL experiments. (An extended version, including absolute number of hospitalizations, can be found in Table S5.)

**QHI restriction is necessary for the standard RL algorithms to perform well** Several counterfactual policies perform worse than NWS (as indicated by negative median differences in returns): RANDOM, BASIC.NWS, and the RL models without the QHI restriction. By contrast, the RL models with the QHI restriction perform significantly better than NWS, as indicated by their significant positive median difference in returns. A rough estimate if A2C.QHI were implemented as-is across all counties in the U.S. (using the Medicare population from 2011, the midpoint of our study period) is that we could see a reduction of 222 NOHR hospitalizations per year (approximate 95% CI = (-491, 1131); details of this CI calculation are in Appendix F). Discussion of this absolute benefit to public health is in Appendix G.

**The futility of including future information** Across both plain and QHI-restricted models, TRPO was the only one that benefited from including future information in the state

Policy	Median Difference	WMW	P-value
*TOPK	0.022	406	0.0002
RANDOM	-0.015	177	0.88
BASIC.NWS	-0.286	30	1.0
AA.QHI	0.03	348	0.0025
DQN	-0.123	43	0.99995
QRDQN	-0.117	51	0.99991
TRPO	-0.065	97	0.99742
A2C	-0.063	100	0.99689
DQN.QHI	0.03	370	0.00242
QRDQN.QHI	0.035	344	0.01121
TRPO.QHI	0.038	338	0.0154
A2C.QHI	<b>0.042</b>	344	0.01121
DQN.F	-0.417	40	0.99996
QRDQN.F	-0.42	48	0.99993
TRPO.F	-0.062	103	0.99625
A2C.F	-0.063	101	0.99669
DQN.QHI.F	-1.895	1	1
QRDQN.QHI.F	0.014	238	0.45904
TRPO.QHI.F	<b>0.046</b>	345	0.01062
A2C.QHI.F	0.036	343	0.01183
DET.TRPO.QHI	-0.662	57	0.99985
DET.A2C.QHI	-0.886	90	0.99837
DET.TRPO.QHI.F	<b>0.032</b>	271	0.21723
DET.A2C.QHI.F	0.02	287	0.13335

Table 1: Comparison between the average return of each counterfactual policy and that of the NWS policy on the evaluation years, summarized across counties (e.g. “Median Diff.” is the median difference in average return). WMW is the Wilcoxon-Mann-Whitney statistic (higher is better); its associated p-value is also included. The first policy, marked by \*, requires oracle knowledge of the future weather.

space. While A2C was minimally impacted, QRDQN and DQN were made noticeably worse. The latter may be due to the future information dramatically increasing the size of the state space/neural network parameters, which our hyper-parameter tuning did not fully counteract. Note that for the TRPO models, the benefit observed with the use of future information would likely be smaller in practice due to forecast / prediction error—the simulation of which is beyond the scope of this paper. Therefore, we focus on the RL models without future information in the remainder of this text.

**The need for stochastic policies** Interpreting policies from the TRPO and A2C models deterministically fails in the heat alerts setting under our rewards model. Additional discussion of this result is in Appendix H.2. This finding raises the question: *Are stochastic policies palatable from a domain perspective?* On the one hand, it is less immediately satisfying that some aspect of heat alerts issuance would be left to chance. On the other hand, in the context of human-in-the-loop decision making—which would likely be the case for public organizations such as NWS (Stuart et al. 2022)—an algorithm reporting probabilities is more informative than reporting only a binary action. In any case, if in the future a heat alerts RL model was running continuously online, it would likely need to utilize exploration (incorporating some randomness into its actions) to update itself over time.

**Comparing policies that perform significantly better than NWS** We note that the performance and behavior of DQN.QHI is practically identical to AA.QHI—not just in its numerical summary, but also in its policy behavior. QRDQN.QHI performs a bit better than DQN.QHI, but not as well as the stochastic policies. Between those, A2C.QHI performs better than TRPO.QHI, though their policies tend to display similar characteristics. Therefore, we focus on A2C.QHI as the best RL policy in the post-hoc analysis. The non-RL counterfactual policies that perform well are that of always issuing an alert on days above an optimized QHI threshold (AA.QHI) and of issuing alerts on the  $b$  hottest days of the summer (TOPK). We note that the ordering of the Wilcoxon-Mann-Whitney statistics for TOPK, AA.QHI, and A2C.QHI is opposite the ordering of these policies’ median difference in returns (compared to NWS). This is due to the longer tails of the A2C.QHI differences, as illustrated in Figure 4. For interpreting these results, recall that TOPK is an oracle policy. However, AA.QHI is an implementable alternative to A2C.QHI, so we must consider it more seriously.

#### 5.4 Post-hoc Contrastive Explanation

To characterize differences between the best RL policies, the NWS policy, and alternative baselines, we consider both stationary features included upstream in the analysis (e.g., climate region and median household income) as well as characteristics of both the NWS and counterfactual alert policies, namely the distributions of the days of summer on which alerts are issued and the lengths of alert streaks (sequences of repeated alerts). We start with these alert characteristics, descriptive histograms of which are in Figure S7. Both A2C.QHI and AA.QHI tend to issue heat alerts earlier in the summer than NWS. A2C.QHI also tends to issue shorter streaks of alerts (i.e., fewer consecutive days of alerts), which makes sense given its ability to learn sequential dependence encoded by the rewards model.

Figure 4 illustrates the varying performance of TOPK, AA.QHI, and A2C.QHI relative to the NWS policy, across climate regions and counties. Note that large heterogeneity in the health effects of heat alert intervention across counties is consistent with previous findings (Wu et al. 2023). A striking visual pattern is the increasing vertical spread from left to right: TOPK performs the least heterogeneously across counties, followed by AA.QHI, and finally A2C.QHI. Similarly, the humid climate regions display more heterogeneity across counties than the others, across all the policies. This is partially due to those regions being larger and thus overrepresented among our 30 counties (see Table S3), but that does not fully explain the discrepancy.

To structure our investigation of why some counties see smaller (or even no) benefits from the application of the heat alerts RL, we fit CART on both the numeric difference in average return (compared to NWS) and a polytomous indicator of which policy performed the best. To prevent CART overfitting to our 30 counties and to facilitate interpretation, we ensure that the minimum number of counties in each leaf (terminal) node is greater than or equal to five for the regression and three for the polytomous classification.

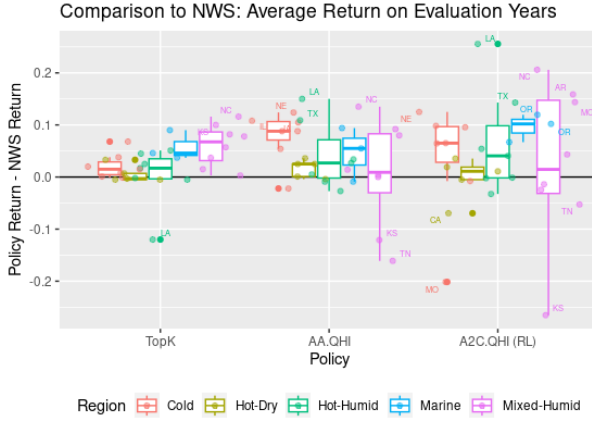


Figure 4: Different policies’ average return relative to NWS across different climate regions, over the evaluation years. Outlier points are labeled with their state abbreviation. Note that TOPK is an oracle policy.

**RL performs best in counties with larger heat alert-health signal and longer heat waves** A classification tree distinguishing A2C.QHI, AA.QHI, NWS, and TRPO.QHI is shown in Figure S8. The most predictive feature of the counterfactual policies’ performance relative to NWS is the size of the alert budget. The fact that the other policies find it harder to improve on NWS with more alerts may be because in such settings it is less critical to discriminate days when heat alerts will be most effective, given that our rewards model assumes more alerts never hurt in an absolute sense. The second split in the tree indicates that the RL performs best when there is greater variation in alert effectiveness across days, in other words, when there is more signal in the heat alert-health relationship that can be leveraged by the RL. The third split highlights how it is better to use RL in counties that tend to experience more prolonged heat waves, which cause AA.QHI to issue more alerts in a row, increasing the likelihood of alert fatigue. Running the same polytymous classification on a set of more conventional covariates (Figure S9), we see a nearly-identical tree except with median household income in place of alert effectiveness and humidity in place of prolonged heat waves. Both of these associations make sense from a domain science perspective.

**Additionally, RL performs better than NWS earlier in the summer** Conducting regression on the difference in average returns between A2C.QHI and NWS using CART (shown in Figure S10) generated complementary insights. The most predictive feature is the median day of summer on which the RL issued heat alerts: A2C.QHI performs better in counties for which it identified that it is optimal to issue alerts earlier in the summer. Whereas, in counties for which it is optimal to issue alerts later in the summer, there was less room for improvement by the RL because the NWS already tends to issue alerts later in the summer.

## 6 Conclusion and Future Work Directions

This work lays the foundation of SDM for climate & health, by (1) formulating and building an SDM pipeline to optimize heat alert issuance, via integrating traditional statistical methods with cutting-edge RL techniques, and (2) offering insights into scenarios where RL improves vs. fails to improve on the observed policy or simpler alternatives.

Ultimately, we found that it was necessary to restrict alerts to days with higher QHI for standard RL algorithms (DQN, QRDQN, TRPO and A2C) to be effective. Our post-hoc analysis enabled investigation of where RL performed better than the NWS policy and the simpler alternative AA.QHI. Future work might explore the use of methods which ensure a new policy is never worse than the existing policy, such as safe policy learning or model predictive control. Alternatively, we could develop a preliminary predictive model to select counties that are likely to benefit from RL, using intuitions similar to those in our CART analysis.

We anticipate several common questions about our approach. The first is how to move beyond a fixed alert budget, important in a changing system (under climate change, the number of extreme heat events is expected to increase). From a practical standpoint, real monetary budgets from stakeholders could be used, for instance “how many times can we afford to open our cooling center(s) this summer?” Future work could also explore modeling alert fatigue as part of the RL environment, for instance by incorporating tools from behavioral science. RL algorithms that are intentionally robust to distribution shift also merit investigation in a climate & health setting.

A second question is whether offline (batch) RL methods, which use only observed data in place of a simulator, could be used to circumvent dependence on the specification of a rewards model. Several major challenges stand in the way of an offline approach, highlighted in our heat alerts example. First, there is a tension between trying to improve the observed policy and controlling distribution shift (Levine et al. 2020): for instance, we see that NWS often issues alerts in streaks, making it hard for offline RL to learn and optimize the impact of an individual alert. Second, assessing the performance of offline RL using off-policy evaluation methods is made difficult by long episodes, large potential for distribution shift (especially in the absence of a modification such as restricting alerts to very hot days), and high degree of autocorrelation in the reward (Uehara, Shi, and Kallus 2022).

We close with a broader view of climate & health decision making. Ideally, an optimal heat alert system would account for different types of health impacts experienced by different demographic groups—future work could explore multi-objective RL. Similarly, it is important to recognize that the issuance of heat alerts is only a first step in reducing the public health impacts of extreme heat (Errett et al. 2023): there is much more work to be done analyzing and expanding local actions in response to heat alerts. If such on-the-ground interventions are able to increase the effectiveness of heat alerts, then this is likely to increase the ability of SDM methods such as RL to identify these effects and help us continue improving our strategies in the future.

## References

Agarwal, A.; Alomar, A.; Alumootil, V.; Shah, D.; Shen, D.; Xu, Z.; and Yang, C. 2021. PerSim: Data-Efficient Offline Reinforcement Learning with Heterogeneous Agents via Personalized Simulators. In *Advances in Neural Information Processing Systems*, volume 34, 18564–18576. Curran Associates, Inc.

Anderson, G. B.; and Bell, M. L. 2011. Heat Waves in the United States: Mortality Risk during Heat Waves and Effect Modification by Heat Wave Characteristics in 43 U.S. Communities. *Environmental Health Perspectives*, 119(2): 210–218.

Anenberg, S. C.; Haines, S.; Wang, E.; Nassikas, N.; and Kinney, P. L. 2020. Synergistic health effects of air pollution, temperature, and pollen exposure: a systematic review of epidemiological evidence. *Environmental Health*, 19: 130.

Austin, P. C. 2017. A tutorial on multilevel survival analysis: methods, models and applications. *International Statistical Review*, 85(2): 185–203.

Bobb, J. F.; Obermeyer, Z.; Wang, Y.; and Dominici, F. 2014. Cause-Specific Risk of Hospital Admission Related to Extreme Heat in Older Adults. *JAMA*, 312(24): 2659–2667.

Carrara, N.; Leurent, E.; Laroche, R.; Urvoy, T.; Maillard, O.-A.; and Pietquin, O. 2019. Budgeted reinforcement learning in continuous state space. *Advances in Neural Information Processing Systems*, 32.

Cutler, M. J.; Marlon, J. R.; Howe, P. D.; and Leiserowitz, A. 2018. The Influence of Political Ideology and Socioeconomic Vulnerability on Perceived Health Risks of Heat Waves in the Context of Climate Change. *Weather, Climate, and Society*, 10(4): 731–746.

Ebi, K. L.; Capon, A.; Berry, P.; Broderick, C.; de Dear, R.; Havenith, G.; Honda, Y.; Kovats, R. S.; Ma, W.; Malik, A.; Morris, N. B.; Nybo, L.; Seneviratne, S. I.; Vanos, J.; and Jay, O. 2021. Hot weather and heat extremes: health risks. *The Lancet*, 398(10301): 698–708.

Ebi, K. L.; Teisberg, T. J.; Kalkstein, L. S.; Robinson, L.; and Weimer, R. F. 2004. Heat Watch/Warning Systems Save Lives: Estimated Costs and Benefits for Philadelphia 1995–98. *Bulletin of the American Meteorological Society*, 85(8): 1067–1074.

Efroni, Y.; Foster, D. J.; Misra, D.; Krishnamurthy, A.; and Langford, J. 2022. Sample-efficient reinforcement learning in the presence of exogenous information. In *Conference on Learning Theory*, 5062–5127.

Efroni, Y.; Misra, D.; Krishnamurthy, A.; Agarwal, A.; and Langford, J. 2024. Provable RL with exogenous distractors via multi-step inverse dynamics. *ICML Workshop on Reinforcement Learning Theory*.

Errett, N. A.; Hartwell, C.; Randazza, J. M.; Nori-Sarma, A.; Weinberger, K. R.; Spangler, K. R.; Sun, Y.; Adams, Q. H.; Wollenius, G. A.; and Hess, J. J. 2023. Survey of extreme heat public health preparedness plans and response activities in the most populous jurisdictions in the United States. *BMC public health*, 23(1): 811.

Frank, J.; Mannor, S.; and Precup, D. 2008. Reinforcement learning in the presence of rare events. In *Proceedings of the 25th international conference on Machine learning*, 336–343.

Guin, S.; and Bhatnagar, S. 2023. A policy gradient approach for finite horizon constrained Markov decision processes. In *2023 62nd IEEE Conference on Decision and Control (CDC)*, 3353–3359. IEEE.

Hammer, M. S.; van Donkelaar, A.; Li, C.; Lyapustin, A.; Sayer, A. M.; Hsu, N. C.; Levy, R. C.; Garay, M. J.; Kalashnikova, O. V.; Kahn, R. A.; Brauer, M.; Apte, J. S.; Henze, D. K.; Zhang, L.; Zhang, Q.; Ford, B.; Pierce, J. R.; and Martin, R. V. 2020. Global Estimates and Long-Term Trends of Fine Particulate Matter Concentrations (1998–2018). *Environmental Science & Technology*, 54(13): 7879–7890. Publisher: American Chemical Society.

Harpole, A.; Zingale, M.; Hawke, I.; and Chegini, T. 2019. pyro: a framework for hydrodynamics explorations and prototyping. *Journal of Open Source Software*, 4(34): 1265.

Hawkins, M. D.; Brown, V.; and Ferrell, J. 2017. Assessment of NOAA National Weather Service Methods to Warn for Extreme Heat Events. *Weather, Climate, and Society*, 9(1): 5–13.

Heo, S.; Bell, M. L.; and Lee, J.-T. 2019. Comparison of health risks by heat wave definition: Applicability of wet-bulb globe temperature for heat wave criteria. *Environmental Research*, 168: 158–170.

Heuillet, A.; Couthouis, F.; and Díaz-Rodríguez, N. 2021. Explainability in deep reinforcement learning. *Knowledge-Based Systems*, 214: 106685.

Hondula, D. M.; Meltzer, S.; Balling, R. C.; and Iñiguez, P. 2022. Spatial Analysis of United States National Weather Service Excessive Heat Warnings and Heat Advisories. *Bulletin of the American Meteorological Society*, 103(9): E2017–E2031. Publisher: American Meteorological Society Section: Bulletin of the American Meteorological Society.

Laber, E. B.; Wu, F.; Munera, C.; Lipkovich, I.; Colucci, S.; and Ripa, S. 2018. Identifying optimal dosage regimes under safety constraints: An application to long term opioid treatment of chronic pain. *Statistics in Medicine*, 37(9): 1407–1418. eprint: <https://onlinelibrary.wiley.com/doi/pdf/10.1002/sim.7566>.

Lee, J. N.; Agarwal, A.; Dann, C.; and Zhang, T. 2023. Learning in POMDPs is Sample-Efficient with Hindsight Observability. ArXiv:2301.13857 [cs, stat].

Levine, A.; Stone, P.; and Zhang, A. 2024. Multistep Inverse Is Not All You Need. *Workshop on Reinforcement Learning Beyond Rewards at the Reinforcement Learning Conference*.

Levine, S.; Kumar, A.; Tucker, G.; and Fu, J. 2020. Offline Reinforcement Learning: Tutorial, Review, and Perspectives on Open Problems. arXiv:2005.01643 [cs, stat]. ArXiv: 2005.01643.

Li, Y.; Zheng, Y.; and Yang, Q. 2018. Dynamic Bike Reposition: A Spatio-Temporal Reinforcement Learning Approach. In *Proceedings of the 24th ACM SIGKDD International Conference on Knowledge Discovery & Data Mining*, 1724–1733. London United Kingdom: ACM. ISBN 978-1-4503-5552-0.

Liao, P.; Greenwald, K.; Klasnja, P.; and Murphy, S. 2020. Personalized HeartSteps: A Reinforcement Learning Algorithm for Optimizing Physical Activity. *Proceedings of the ACM on Interactive, Mobile, Wearable and Ubiquitous Technologies*, 4(1): 18:1–18:22.

Masselot, P.; Chebana, F.; Campagna, C.; Lavigne, E.; Ouarda, T. B.; and Gosselin, P. 2021. Machine Learning Approaches to Identify Thresholds in a Heat-Health Warning System Context. *Journal of the Royal Statistical Society Series A: Statistics in Society*, 184(4): 1326–1346.

Microsoft AI for Good Research Lab. 2021. U.S. Broadband Usage Percentages Dataset.

MIT Election Data and Science Lab. 2018. County Presidential Election Returns 2000–2020.

Mu, T.; Theocharous, G.; Arbour, D.; and Brunskill, E. 2021. Constraint Sampling Reinforcement Learning: Incorporating Expertise For Faster Learning. ArXiv:2112.15221 [cs].

Nahum-Shani, I.; Smith, S. N.; Spring, B. J.; Collins, L. M.; Witkiewitz, K.; Tewari, A.; and Murphy, S. A. 2017. Just-in-Time Adaptive Interventions (JITAIs) in Mobile Health: Key Components and Design Principles for Ongoing Health Behavior Support.

*Annals of Behavioral Medicine: A Publication of the Society of Behavioral Medicine*, 52(6): 446–462.

Narayanan, S.; Lage, I.; and Doshi-Velez, F. 2022. (When) Are Contrastive Explanations of Reinforcement Learning Helpful? ArXiv:2211.07719 [cs].

Ng, C. F. S.; Ueda, K.; Takeuchi, A.; Nitta, H.; Konishi, S.; Bagrowicz, R.; Watanabe, C.; and Takami, A. 2014. Sociogeographic Variation in the Effects of Heat and Cold on Daily Mortality in Japan. *Journal of Epidemiology*, 24(1): 15–24.

Padakandla, S. 2021. A survey of reinforcement learning algorithms for dynamically varying environments. *ACM Computing Surveys (CSUR)*, 54(6): 1–25.

Pearl, J. 2012. The mediation formula: A guide to the assessment of causal pathways in nonlinear models. *Causality: Statistical perspectives and applications*, 151–179.

Puiutta, E.; and Veith, E. M. 2020. Explainable Reinforcement Learning: A Survey. ArXiv:2005.06247 [cs, stat].

Puterman, M. L. 2014. *Markov decision processes: discrete stochastic dynamic programming*. John Wiley & Sons.

Raffin, A.; Hill, A.; Gleave, A.; Kanervisto, A.; Ernestus, M.; and Dormann, N. 2021. Stable-Baselines3: Reliable Reinforcement Learning Implementations. *Journal of Machine Learning Research*, 22(268): 1–8.

Ray, A.; Achiam, J.; and Amodei, D. 2019. Benchmarking Safe Exploration in Deep Reinforcement Learning. Technical report, OpenAI.

Romoff, J.; Henderson, P.; Piche, A.; Francois-Lavet, V.; and Pineau, J. 2018. Reward Estimation for Variance Reduction in Deep Reinforcement Learning. In *Conference on Robot Learning*, 674–699. PMLR.

Sinclair, S. R.; Vieira Frujeri, F.; Cheng, C.-A.; Marshall, L.; Barbalho, H. D. O.; Li, J.; Neville, J.; Menache, I.; and Swaminathan, A. 2023. Hindsight Learning for MDPs with Exogenous Inputs. In Krause, A.; Brunskill, E.; Cho, K.; Engelhardt, B.; Sabato, S.; and Scarlett, J., eds., *Proceedings of the 40th International Conference on Machine Learning*, volume 202 of *Proceedings of Machine Learning Research*, 31877–31914. PMLR.

Stuart, N. A.; Hartfield, G.; Schultz, D. M.; Wilson, K.; West, G.; Hoffman, R.; Lackmann, G.; Brooks, H.; Roebber, P.; Bals-Elsholz, T.; Obermeier, H.; Judt, F.; Market, P.; Nietfeld, D.; Telfeyan, B.; DePodwin, D.; Fries, J.; Abrams, E.; and Shields, J. 2022. The Evolving Role of Humans in Weather Prediction and Communication. *Bulletin of the American Meteorological Society*, 103(8): E1720–E1746. Publisher: American Meteorological Society Section: Bulletin of the American Meteorological Society.

Sutton, R. S.; and Barto, A. G. 2018. *Reinforcement Learning: An Introduction*. The MIT Press, second edition.

Sutton, R. S.; McAllester, D.; Singh, S.; and Mansour, Y. 1999. Policy gradient methods for reinforcement learning with function approximation. *Advances in neural information processing systems*, 12.

Tec, M.; Duan, Y.; and Müller, P. 2023. A Comparative Tutorial of Bayesian Sequential Design and Reinforcement Learning. *The American Statistician*, 77(2): 223–233.

Towers, M.; Terry, J. K.; Kwiatkowski, A.; Balis, J. U.; Cola, G. d.; Deleu, T.; Goulão, M.; Kallinteris, A.; KG, A.; Krimmel, M.; Perez-Vicente, R.; Pierré, A.; Schulhoff, S.; Tai, J. J.; Shen, A. T. J.; and Younis, O. G. 2023. Gymnasium.

Tzikas, D. G.; Likas, A. C.; and Galatsanos, N. P. 2008. The variational approximation for Bayesian inference. *IEEE Signal Processing Magazine*, 25(6): 131–146.

Uehara, M.; Shi, C.; and Kallus, N. 2022. A Review of Off-Policy Evaluation in Reinforcement Learning. ArXiv:2212.06355 [cs, math, stat].

U.S. Census Bureau. 2014. 2009–2013 American Community Survey 5-year County-level Estimates of Population and Median Household Income.

U.S. Energy Information Administration. 2020. Climate Zones - DOE Building America Program.

van der Waa, J.; van Diggelen, J.; Bosch, K. v. d.; and Neerincx, M. 2018. Contrastive Explanations for Reinforcement Learning in terms of Expected Consequences. ArXiv:1807.08706 [cs, stat].

Weinberger, K. R.; Wu, X.; Sun, S.; Spangler, K. R.; Nori-Sarma, A.; Schwartz, J.; Requia, W.; Sabath, B. M.; Braun, D.; Zanobetti, A.; Dominici, F.; and Wellenius, G. A. 2021. Heat warnings, mortality, and hospital admissions among older adults in the United States. *Environment International*, 157: 106834.

Weinberger, K. R.; Zanobetti, A.; Schwartz, J.; and Wellenius, G. A. 2018. Effectiveness of National Weather Service heat alerts in preventing mortality in 20 US cities. *Environment International*, 116: 30–38.

Wu, Q.; Chen, X.; Zhou, Z.; Chen, L.; and Zhang, J. 2021. Deep Reinforcement Learning With Spatio-Temporal Traffic Forecasting for Data-Driven Base Station Sleep Control. *IEEE/ACM Transactions on Networking*, 29(2): 935–948.

Wu, X.; Weinberger, K. R.; Wellenius, G. A.; Dominici, F.; and Braun, D. 2023. Assessing the causal effects of a stochastic intervention in time series data: are heat alerts effective in preventing deaths and hospitalizations? *Biostatistics*.

Xu, H.; Zhan, X.; and Zhu, X. 2022. Constraints Penalized Q-learning for Safe Offline Reinforcement Learning. ArXiv:2107.09003 [cs].

Zajonc, T. 2012. Bayesian Inference for Dynamic Treatment Regimes: Mobility, Equity, and Efficiency in Student Tracking. *Journal of the American Statistical Association*, 107(497): 80–92.

Zanobetti, A.; O'Neill, M. S.; Gronlund, C. J.; and Schwartz, J. D. 2013. Susceptibility to Mortality in Weather Extremes: Effect Modification by Personal and Small Area Characteristics In a Multi-City Case-Only Analysis. *Epidemiology (Cambridge, Mass.)*, 24(6): 809–819.

## Appendix

### A Heat Alerts MDP Terminology

Table S1 summarizes the heat alerts MDP components.

### B Details of the Data Set

Evidence from the climate & health and environmental epidemiology literature guides our selection of relevant variables as well as feature engineering.

#### B.1 Heat Index and Heat Alerts

We follow Weinberger et al. (2021) and Wu et al. (2023) in using population-weighted maximum heat index to describe heat exposure in each county. They also combined NWS heat “warnings” and “advisories” into the single category of “alerts”. In some locations, where the forecast zones in which the NWS issues alerts are smaller than county boundaries, the alert history was taken from whichever forecast zone contained the largest proportion of the 2010 county population.

#### B.2 Medicare Hospitalizations

Medicare is available for people aged 65 years and older. The hospitalization claims data we use in this study is from Medicare Part A, fee-for-service. A 2021 report (The Commonwealth Fund 2021) found that fee-for-service enrollees do not significantly differ from managed care enrollees (the rest of the Medicare population).

Figure S1 illustrates the rationale for excluding obviously heat-related hospitalization types from the pooled outcome, as described in section 4.1.

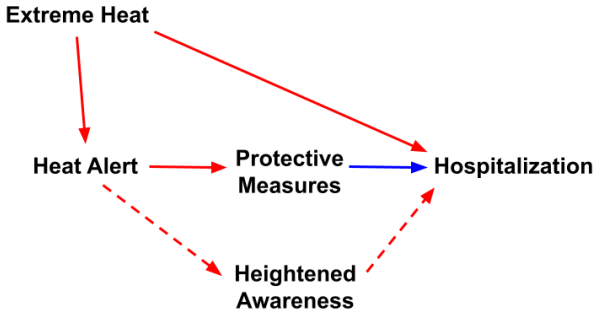


Figure S1: Unobserved mediation of the effect of heat alerts on hospitalizations by heightened awareness.

#### B.3 Descriptive Statistics of Heat, Alerts, and Hospitalizations

Table S2 provides descriptive statistics of the heat alerts dataset, both for the 30 counties in our RL analysis and all the counties with population  $\geq 65,000$  (used to create the BROACH environment). The two sets of statistics are similar aside from the number of heat alerts issued because the counties in the RL analysis were selected specifically for having issued higher numbers of alerts. Other observations

are the long tail of the number of NWS alerts per county-summer, that some heat alerts were issued on days that were not very hot in an absolute or relative (quantile) sense, that there were some county-summers with few “hot” days (90th percentile by county<sup>7</sup>) and others with many, and that the distribution of day-of-summer for NWS heat alerts and 90th percentile QHI by county are quite similar. A few other relevant statistics not shown in the table are that (across all the counties) there were a total of 40,387 heat alerts issued between 2006 and 2016, that 17.2% of NWS heat alerts were issued on days with heat index values that were *not* in their county’s top 90th percentile, and that 74.0% of days in the top 90th QHI by county did not have NWS heat alerts.

### C Details of the Bayesian Rewards Model

Recall our formulation for the expected per capita rate of NOHR hospitalizations at time  $t$  in county-summer  $(k, j)$  when taking action  $a$ :

$$\rho_t^{(k, j)}(a) = \lambda_k(s_t^{(k, j)})(1 - a \cdot \tau_k(s_t^{(k, j)}))$$

**The baseline and effectiveness functions** Note that  $\lambda_k$  and  $\tau_k$  are unique to each location  $k$ , allowing for spatial heterogeneity and thus reducing the possibility of unobserved spatial confounding (Bell and Jones 2015; Nobre, Schmidt, and Pereira 2021; Tec et al. 2024). However, this design introduces the challenge of estimating these functions under limited data for each county (11 summers between 2006 and 2016). This challenge is amplified by the low signal in the health effects of heat and heat alerts (Weinberger et al. 2021). To address this, we adopt a (generalized) linear model for  $\lambda_k$  and  $\tau_k$  paired with (i) borrowing statistical strength across counties using a data-driven random effects prior and (ii) injecting domain knowledge on the signs of certain coefficients. The functions  $\lambda_k$  and  $\tau_k$  are specified as

$$\begin{aligned} \lambda(s_t^{(k, j)}) &:= \exp\left(\beta_k^\top s_t^{(k, j)}\right), \\ \tau(s_t^{(k, j)}) &:= \text{sigmoid}\left(\delta_k^\top s_t^{(k, j)}\right), \end{aligned} \quad (5)$$

where  $\beta_k$  and  $\delta_k$  are the model coefficients for each county  $k \in \mathcal{K}$ . While this specification is a linear combination of state variables, we allow for non-linear effects by using a piecewise linear basis expansion on the quantile of heat index (QHI) and a spline basis on the day of summer. The piecewise linear expansion on QHI in  $\lambda$  (the baseline function) has knots at the 25th and 75th percentiles. In  $\tau$  (the alert effectiveness function), we include only a linear term for QHI—again, conditional on day of summer and excess QHI (compared to the average of the last 3 days, a time window informed by the literature on heat waves and health (Metzger, Ito, and Matte 2010))—to both stabilize effect identification and facilitate interpretation. The spline on day of

<sup>7</sup>Here, the 90th percentile was chosen to provide some intuition for the distribution of heat index and heat alerts. For context, Hondula et al. (2022) found that 95th percentile daily maximum heat index was the climatological indicator most strongly correlated with NWS heat alert frequency.

RL Term	Notation	Meaning in the Heat Alerts Application
episode	$t \in \{0, \dots, H-1\}$	the $H = 152$ days of the warm season/summer in a specific year and county; $H$ is the horizon
state	$s_t = (\xi_t, x_t)$	a vector of time-varying factors influencing the effect of heat on hospitalizations and the effectiveness of an alert; $\xi_t$ is the exogenous component (e.g., heat index) and $x_t$ is the endogenous component (e.g., history of heat alerts)
action	$a_t$	whether a heat alert is issued (1) or not (0) at time $t$
reward	$r_t = R(s_t, a_t)$	daily rate of heat-related hospitalizations at time $t$ ; a negative sign transform is applied so that fewer hospitalizations corresponds to a greater reward
agent	—	the algorithmic decision-maker that implements a policy to determine when to issue heat alerts
policy	$\pi(a_t   s_t)$	the heat alert issuance rule; the NWS policy is the rule that was used to issue heat alerts in the U.S. from 2006-2016
cumulative reward / return	$\sum_{h=t}^{H-1} r_h$	sum of remaining reward (transformed hospitalizations) at time $t$ ; unless otherwise specified, “cumulative” implies $t = 0$
intervention / alert budget	$\sum_{t=0}^{H-1} a_t \leq b$	the maximum number of heat alerts that can be issued in a given county-summer; in our experiments, the observed number of NWS alerts

Table S1: MDP/RL terminology in the context of the heat alerts environment.

Variable	Min.	Q1	Median	Mean	Q3	Max.
*NOHR hosps per 1,000	5.4 (3.1)	12.5 (12.7)	14.8 (15.2)	15 (15.3)	17.3 (17.8)	25.7 (34.5)
*No. of NWS alerts	0 (0)	4 (0)	8 (3)	9.6 (4.8)	13 (7)	43 (57)
DMHI on alert days (°F)	70.5 (68.3)	100.3 (99.7)	103.5 (103.2)	102.5 (102.6)	106.2 (105.9)	121.1 (144)
Q-DMHI on alert days	18.9 (15.6)	91.6 (92.6)	95.8 (96.9)	93.4 (94.2)	98.2 (98.9)	100 (100)
*No. of 90th pct. HI days	0 (0)	9 (8)	14 (14)	15.4 (15.4)	21 (21)	46 (61)
DOS of NWS alerts	16 (2)	68 (69)	84 (84)	83.4 (83.5)	99 (99) (150)	142
DOS of 90th pct. HI days	15 (1)	72 (69)	88 (85)	86.9 (85.2)	102 (102)	145 (153)

Table S2: Summary statistics for our 30 counties of interest (and all the counties) of Medicare NOHR hospitalizations, NWS heat alerts, heat index, and day of summer for several features of interest. DMHI = daily maximum heat index, Q-DMHI = county quantile of DMHI (referred to simply as QHI in the main text), DOS = day of summer (out of 152). Variables given per county-summer are marked with \*.

summer (with 3 degrees of freedom) is included in both  $\lambda$  and  $\tau$ .

Figure S2 illustrates the interaction of  $\lambda_k$  and  $\tau_k$  to capture the total effect of heat alerts on NOHR hospitalizations. For instance, we see that in early summer it is possible to have high heat alert effectiveness even when the heat index is not as high as it is later in the summer, possibly because people are less well-adapted to heat and/or more responsive to heat alerts early on.

**Data-driven prior** We propose a data-driven prior distribution that allows borrowing statistical strength from other locations while preserving the possibility of spatial heterogeneity. Let  $w_k$  denote the vector of county-level features that are not included in the state vector but are predictive of the effect of heat and heat alerts on hospitalizations (see “County-level characteristics” in 4.1), and let  $\gamma_k = [\beta_k; \delta_k] = (\gamma_k^\ell)_{\ell=1}^L$  denote the parameters corresponding to county  $k$ . Let  $N()$  denote a normal distribution.

Then, the prior distribution of each  $\gamma_k^\ell$  is set independently as  $p_\theta(\gamma_k^\ell | \sigma_\ell, w_k) =$

$$\begin{cases} N(\gamma_k^\ell; f_\theta(w_k)_\ell, \sigma_\ell^2) & \text{no domain knowledge,} \\ \text{LogN}(\gamma_k^\ell; \exp(f_\theta(w_k)_\ell), \sigma_\ell^2) & \text{if } \gamma_k^\ell \in (0, \infty), \\ \text{NegLogN}(\gamma_k^\ell; -\exp(f_\theta(w_k)_\ell), \sigma_\ell^2) & \text{if } \gamma_k^\ell \in (-\infty, 0) \end{cases} \quad (6)$$

where  $f_\theta$  is a feed-forward neural network (with weights  $\theta$  and  $L$  outputs) specifying the prior mean as a function of the spatial features, and  $\sigma_\ell$  specifies the prior scale. We use a standard hyper-prior  $p(\sigma_\ell) = \text{HalfCauchy}(\sigma_\ell)$  (Gelman 2006).

The domain knowledge constraints we utilize are: (i) past heat alerts cannot increase the baseline hospitalization rate—in other words, alert fatigue can be identified only in  $\tau$ —and (ii) higher QHI cannot decrease the effectiveness of heat alerts—note that this is conditional on day of summer.

The weights  $\theta$  are learned from the data to characterize

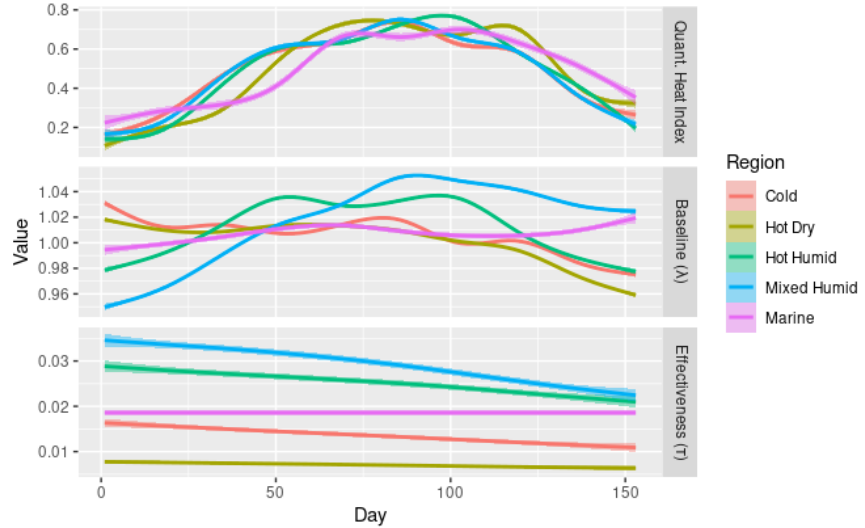


Figure S2: Smoothed trajectories of observed quantile of heat index, modeled baseline NOHR hospitalization rate, and modeled alert effectiveness (assuming no past alerts) across days of summer; colored by climate region. Note that  $\lambda$  and  $\tau$  are normalized as they are in the RL reward function.

the prior distribution that best describes the latent space according to the data. As remarked in (Wang, Miller, and Blei 2019), this procedure can be seen as a form of Empirical Bayes. According to this viewpoint, we can interpret the prior mean function  $f_\theta$  in equation 6 as an encoder that maps the county-level features  $w_k$  to a data-driven probability distribution over a latent space. The coefficients  $\gamma_k$  are latent variables in this space. The predictive model  $\rho_t^{(k,j)}(a)$  in equation 4 acts as a decoder.

**Training** Traditional Bayesian inference methods using Markov Chain Monte Carlo are computationally prohibitive for our model due to the high dimensionality of parameters and the number of observations for each county. To address this issue, we use variational inference, which introduces an approximation of the true posterior distribution of the model parameters. We summarize the approach.

Let  $(\gamma, \sigma) \sim q_\psi$  denote an approximation of the true posterior distribution where  $\psi$  are the learnable parameters of the approximating distribution  $q_\psi$ . Next, let  $o_t^{(k,j)} = (s_t^{(k,j)}, a_t^{(k,j)}, y_t^{(k,j)}, n^{(k,j)})$  denote a data point in the training set and  $\mathcal{L}(o_t^{(k,j)}; \gamma_k)$  be the Poisson log-likelihood corresponding to this data point (see equation 4). Variational inference attempts to maximize the likelihood of the observed data while penalizing the divergence between the variational posterior  $q_\psi$  and the prior  $p_\theta(\gamma, \sigma|w) = \prod_{k,l} p_\theta(\gamma_k^l|\sigma_\ell, w_k) \prod_l p(\sigma_\ell)$ . The optimization objective is to maximize the evidence lower bound (ELBO) given by

$$\text{ELBO}(\psi, \theta) = \mathbb{E}_{q_\psi} \left[ \sum_{k,j,t} \mathcal{L}(o_t^{(k,j)}; \gamma_k) \right] - D_{\text{KL}}(q_\psi(\gamma, \sigma) \parallel p_\theta(\gamma, \sigma|w)), \quad (7)$$

where  $D_{\text{KL}}$  denotes the Kullback-Leibler divergence. To ensure the variational posterior is flexible enough to approxi-

mate the true posterior, we use a low-rank multivariate normal distribution (Tomczak, Swaroop, and Turner 2020). This approach uses a bijective transform of the parameters to an unconstrained space and then applies a low-rank factorization to the covariance matrix of the multivariate normal distribution. Thereby, it allows for efficient computation while approximating the true correlation structure of the joint posterior distribution. The data-driven prior parameters  $\theta$  are learned jointly with the variational parameters  $\psi$  using stochastic optimization. Specifically, we train one neural network for  $\beta$  (the coefficients of the baseline function) and another for  $\delta$  (the coefficients of the alert effectiveness function). Both networks have one hidden layer with 32 units—this modest architecture avoids overfitting the relatively small number of spatial features in our dataset.

**Results** The rewards model clearly converged in its loss across epochs (shown in Figure S3) and achieved higher predictive accuracy than standard machine learning algorithms (i.e., random forest and neural network). Predicting the rate of NOHR hospitalizations in the Medicare population in each county, this model has  $R^2 = 0.102$ —using the calculation  $SSR/SST$  for comparability with earlier machine learning models (such as that we used when checking the signal in the mortality data). Predicting the absolute number of NOHR hospitalizations, it has  $R^2 = 0.884$ —much higher because the value is mostly driven by county population size. The model also displayed very good coverage when we ran it on synthetic data (1,000 samples from the posterior predictive) using known coefficients: average coverage across parameters for a 90% CI was 0.897.

Figure S4 shows one posterior sample across the 761 counties on which the model was fit. Note that the spread across counties is larger than the spread within counties, so the IQR bars are no larger for multiple samples. Overall, we

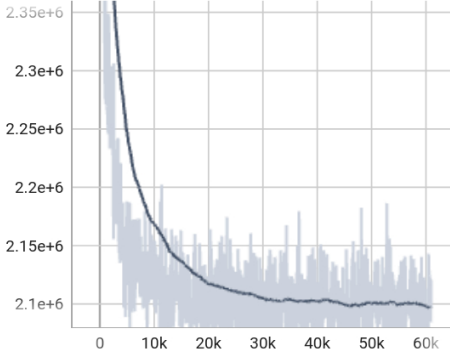


Figure S3: Convergence of the ELBO in the Bayesian rewards model during training (80 epochs).

see that the coefficients on past alerts in today's alert effectiveness ( $\tau$ ) are both negative, empirical evidence of alert fatigue. In the baseline hospitalization rate ( $\lambda$ ), we see a strong protective effect by weekend.

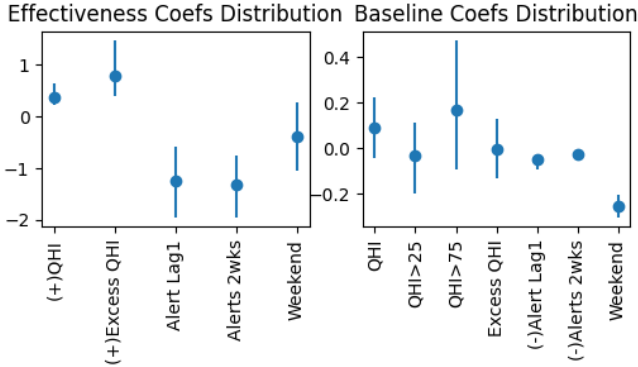


Figure S4: A sample of posterior coefficients from the rewards model (in  $\tau$  and  $\lambda$  respectively), displaying IQR and median. Bias and coefficients for the spline on day of summer are not shown, for ease of interpretability. (+)/(-) indicates a coefficient constrained to be positive/negative.

## D Details of the RL Analysis

### D.1 Selection of 30 Counties

Out of the 170 counties with 75 or more heat alerts issued between 2006 and 2016, we selected 30 using the following criteria: for each climate region<sup>8</sup>, select the county with the highest variance in estimated heat alert effectiveness (indicating higher signal as identified by our rewards model). To get up to 30, repeat this selection, but first prioritize selecting a county from a U.S. state not already in the set, and if we must repeat a state, do not select a county that is directly adjacent to one already in the set. If there are no more eligible

<sup>8</sup>Excluding “Mixed Dry” and “Very Cold” because there were very few counties in these regions with sufficient population size

counties in a region, select from a larger region. Characteristics of these 30 counties are provided in Table S3.

### D.2 RL Algorithm Descriptions

DQN is standard Deep Q-learning. QRDQN differs from DQN in that rather than estimating the average return from taking action  $a$  at state  $s$ , it estimates the distribution over the returns using quantile regression. Compared to other common stochastic policy gradient algorithms, TRPO is distinguished by its constraint on the size of the optimization step, so that the new policy lies within a “trust region” from the previous policy, in which local approximations of the policy function are still accurate (Han et al. 2023). A2C improves on the basic setup of actor-critic by updating its policy model using the advantage function, which indicates how much better an action is than the alternative(s), rather than just the state-action value of that one action; this helps increase model stability (Han et al. 2023).

### D.3 Hyperparameter Tuning

RL algorithms are known to be sensitive to their hyperparameters, especially in empirical settings (Eimer, Benjamins, and Lindauer 2022). To address this concern, we tuned hyperparameters per county, using the average return metric. First, we did a broad sweep on one county from each of the five climate regions using TRPO.QHI, experimenting with values of learning rate  $\in \{0.01, 0.001, 0.0001\}$ , discount factor  $\in \{1.0, 0.999, 0.99\}$ , neural network architecture (number of hidden layers  $\in \{1, 2, 3\}$  and number of hidden units  $\in \{16, 32, 64\}$ ), and size of the replay buffer  $\in \{1024, 2048, 4096\}$ ; paired with possible QHI thresholds  $\in \{0.55, 0.7, 0.85\}$  and both including and not including future information. After determining that learning rate=0.001 and discount factor=1.0 performed the best across the board, we tuned the remaining parameters for each county and each RL model (all combinations of TRPO, A2C, QRDQN and DQN with and without QHI restrictions and future information). To make the computation time more reasonable, we did a grid search on two values each for the number of hidden layers (2 or 3), number of hidden units (16 or 32), and size of the replay buffer (1,500 or 3,000). For QRDQN specifically, we also tested different values for the number of quantiles, which is closely tied to computation time for this algorithm. Using 10 quantiles rather than 20 ended up being not only faster but also better, potentially due to the latter overfitting.

### D.4 Sensitivity Analysis Using 2014-2016 as the Evaluation Years

For real-world deployment of a heat alert-RL system, an ideal setup would be to train on years  $\{1, \dots, x\}$  and evaluate on year  $x + 1$ . However, in this analysis we held out  $\{2007, 2011, 2015\}$  as the evaluation set to provide a better representation of historical performance. Note that while days within each episode are consecutive, the 7-month gap between episodes lessens concern about correlated episodes.

To provide intuition for how sequential training-testing would look, we re-ran the best RL model (A2C.QHI) using

County Fips (State name abbreviation)	Region	No. Alerts (Eval Years)	Population Density (/mi <sup>2</sup> )	Median HH Income (USD)	Democratic Voters (%)	Broadband Usage (%)	Average PM <sub>2.5</sub> ( $\mu\text{g}/\text{m}^3$ )
5045 (AR)	MxHd	61	179.00	50314.00	34.00	37.50	9.08
20161 (KS)	MxHd	47	120.00	43962.00	43.50	52.20	6.35
21059 (KY)	MxHd	24	212.00	46555.00	38.70	53.30	10.22
29019 (MO)	MxHd	50	242.00	48627.00	51.60	46.60	7.85
37085 (NC)	MxHd	31	200.00	44625.00	39.30	46.70	9.65
40017 (OK)	MxHd	63	133.00	63629.00	22.80	70.10	7.53
47113 (TN)	MxHd	58	176.00	41617.00	44.30	79.40	9.29
42017 (PA)	MxHd	25	1036.00	76555.00	51.00	85.10	9.14
41053 (OR)	Mrn	31	102.00	52808.00	45.60	79.20	3.24
41067 (OR)	Mrn	31	745.00	64180.00	57.70	82.70	4.28
53015 (WA)	Mrn	23	90.00	47596.00	49.40	53.60	3.59
13031 (GA)	HtHd	43	106.00	35840.00	38.90	57.50	9.01
22109 (LA)	HtHd	34	91.00	49960.00	27.90	55.50	8.26
28049 (MS)	HtHd	57	283.00	37626.00	69.90	36.50	8.50
45015 (SC)	HtHd	48	168.00	52427.00	41.20	66.20	8.72
48157 (TX)	HtHd	42	707.00	85297.00	47.80	83.70	8.64
48367 (TX)	HtHd	41	131.00	64515.00	18.30	52.20	7.84
22063 (LA)	HtHd	42	201.00	56811.00	13.70	47.60	8.87
4015 (AZ)	HtDr	29	15.00	39200.00	28.70	63.60	4.59
6025 (CA)	HtDr	40	42.00	41807.00	64.00	64.40	7.22
32003 (NV)	HtDr	29	251.00	52873.00	55.90	78.10	5.21
4013 (AZ)	HtDr	72	423.00	53596.00	44.00	77.40	6.38
6071 (CA)	HtDr	29	103.00	54090.00	51.60	77.10	6.38
17115 (IL)	Cold	22	190.00	46559.00	45.70	63.60	8.87
17167 (IL)	Cold	25	228.00	55449.00	46.00	66.50	8.75
19153 (IA)	Cold	24	764.00	59018.00	54.90	57.90	8.25
19155 (IA)	Cold	27	98.00	51304.00	44.30	42.00	7.89
34021 (NJ)	Cold	29	1639.00	73480.00	67.30	81.60	9.31
29021 (MO)	Cold	44	219.00	44363.00	43.70	48.80	7.97
31153 (NE)	Cold	27	681.00	69965.00	37.60	72.60	7.92

Table S3: Descriptive statistics of the 30 counties used in policy optimization. Climate region abbreviations = {MxHD: Mixed-Humid, Mrn: Marine, HtHd: Hot-Humid, HtDr: Hot-Dry, Cold: Cold}. HH = household. PM<sub>2.5</sub> is an annual average.

Evaluation Period	QHI Median	Median Diff. (RL-NWS)	WMW p-value
Main Analysis:			
{2007, 2011, 2015}	0.042	0.011	
2007	0.51	0.006	0.013
2011	0.555	0.016	0.027
2015	0.519	0.01	0.010
Sensitivity Analysis:			
{2014, 2015, 2016}	0.007	0.121	
2014	0.46	0.002	0.012
2015	0.519	0.009	0.022
2016	0.6	-0.005	0.777

Table S4: Comparison of results using 2014-2016 as the evaluation years (sensitivity analysis) as opposed to 2007,2011,2015 (main analysis).

2006-2013 to train and 2014-2016 to evaluate. To reduce the computational burden, we used the optimized hyperparameters from the main analysis for each county. Table S4 shows

the aggregated results as well as results stratified by year. A few notable results are that (i) the ordering of the original results (2007 < 2015 < 2011) is the same as the ordering of median QHI, (ii) the 2015 results are similar in each evaluation scheme, and (iii) the 2016 result is the worst. However, this last result is overly bleak because in an online deployment we would not be evaluating 3 years ahead—the model would be updated at least once a year.

## E Summary of the Workflow Using BROACH

This section is meant to illustrate a toy example of our workflow. Imagine seven counties located in two climate regions, as shown in the figure below.

Climate Region A				Climate Region B		
1	2	3	4	5	6	7

Let the training years TY = {2006, 2008, 2009, 2010, 2012, 2013, 2014, 2016} and evaluation years EY = {2007, 2011, 2015}.

First, train the rewards model on counties 1-7 and years TY  $\cup$  EY to obtain posterior distributions for  $r_1(s, a), \dots, r_7(s, a)$ . Then, for each county, follow the steps below. Consider county 1 for illustration. Our procedure is as follows:

```

1: if Training RL (with a QHI restriction) then
2:   for h in {0.5, 0.55, ..., 0.9} do
3:     for i in 1 to  $N_T$  episodes do
4:       Sample  $r_{1,i}(s, a)$  from the posterior for
        $r_1(s, a)$ 
5:       Sample  $\xi_i \sim TY \times \{\xi_1, \xi_2, \xi_3, \xi_4\}$ 
6:       Update  $\pi_{1,h}(a|s)$  s.t.  $a = 0$  if QHI < h, using
        $r_{1,i}$  and  $\xi_i$ 
7:     end for
8:     Select  $\pi_{1,h}^*$  (across i) with the largest average re-
       turn using  $\xi_i \sim EY \times \{\xi_2, \xi_3, \xi_4\}$ 
9:   end for
10:  else if Tuning RL or AA.QHI then
11:    for h in {0.5, 0.55, ..., 0.9} do
12:      for i in 1 to  $N_E$  episodes do
13:        Sample  $r_{1,i}(s, a)$  from the posterior for
         $r_1(s, a)$ 
14:        Sample  $\xi_i \sim EY \times \{\xi_2, \xi_3, \xi_4\}$ 
15:        Calculate cumulative reward using  $\pi_{1,h}^*$  (or
        AA.QHI with h),  $r_{1,i}$  and  $\xi_i$ 
16:      end for
17:    end for
18:    Select  $h^*$  with the largest return
19:  else if Final evaluation for any policy (but using notation
  for optimized RL) then
20:    for i in 1 to  $N_E$  episodes do
21:      Sample  $r_{1,i}(s, a)$  from the posterior for  $r_1(s, a)$ 
22:      Sample  $\xi_i \sim EY \times \{\xi_1\}$ 
23:      Calculate cumulative reward using  $\pi_{1,h^*}^*$ ,  $r_{1,i}$ 
      and  $\xi_i$ 
24:    end for
25:  end if

```

## F Approximate Confidence Interval Calculation

To generate an approximate confidence interval for the absolute number of NOHR hospitalizations saved by implementing our best RL model, we use the estimates from the final evaluation for A2C.QHI and NWS. However, rather than first calculating average returns per county (across the 1,000 evaluation episodes) and then taking the median across the 30 counties, we first take the median return (across the 30 counties) from each of the 1,000 evaluation episodes and then calculate the 2.5% and 97.5% quantiles of the resulting distribution of medians.

## G Discussion of Absolute Health Benefits

Do we estimate substantive health benefits from implementing the improved heat alerts policies detailed in the main text? For general context, the median rate of NOHR hospitalizations per 10,000 Medicare enrollees per summer during our study period was 148 (Table S2), and we estimated

that deploying our best RL model *relative to issuing no heat alerts* would save 2 of these 148, or 1.4%, in the 30 counties in our RL analysis. Noting that the overall relative risk of a Medicare enrollee experiencing one of the NOHR hospitalization types on a heat wave day is about 1.10 (Bobb et al. 2014), this is substantial evidence in support of continuing to issue heat alerts to protect public health.

Compared to the observed NWS policy, A2C.QHI applied to the 30 counties in our analysis would save approximately 0.042 NOHR hospitalizations per 10,000 Medicare enrollees per summer, a reduction of only 0.03%. Multiplying this by 49 million, the size of the Medicare population in 2011 (the midpoint of our study period), yields about 222 NOHR hospitalizations saved per summer. However, this modest value should be further contextualized by several points.

Firstly, heat alerts by themselves (and in our case, the re-arrangement of the same number of heat alerts) are a very cost-effective intervention, so even small reductions in health harms are promising.

Secondly, if we take into account the large heterogeneity in the benefit of RL across counties with numbers from the CART regression (Figure S10), assuming that we figure out how to implement a safe policy such that counties which would not benefit are unaffected, this number increases to 262 ((49m/10k)\*(0.074\*0.17 + 0.053\*0.33 + 0.18\*0.13)) NOHR hospitalizations saved per summer. We obtain a nearly identical result from running a CART analysis using only variables which are available for all 761 counties that were included in the rewards model, and applying the results of that model across the whole set of counties. These are rough approximations given that they assume the proportion of counties in which RL alert policies were found to improve health outcomes in our sample is generalizable to the rest of the US. It is plausible that our sample of 30 counties is unrepresentative of the U.S. as they tend to have higher variability in alert effectiveness (increasing potential improvements from RL) and also higher alert budgets.

Thirdly, these metrics reflect the climate and Medicare population between 2006 and 2016. We confidently anticipate that both the frequency of extreme heat events under climate change and the size of the Medicare population will continue increasing (Dahl et al. 2019). For instance, while there were 49 million Medicare enrollees in 2011, by 2023 this number has increased to over 65 million, and by 2050 it is projected to be over 85 million (The Boards of Trustees of the Federal Hospital Insurance and Federal Supplementary Medical Insurance Trust Funds 2023).

Fourthly, the numbers reported in this study should not be interpreted as the overall benefit to public health from improving heat alerts issuance strategies. The health data used in our study only reflect inpatient hospitalizations from NOHR causes billed to Medicare Part A, or hospital fee-for-service. Only about 60% of Medicare enrollees are in the fee-for-service population<sup>9</sup>, so hospitalizations of the other 40% do not appear in our dataset.

<sup>9</sup>[https://www.cms.gov/Research-Statistics-Data-and-Systems/Statistics-Trends-and-Reports/Beneficiary-Snapshot/Downloads/Bene\\_Snapshot.pdf](https://www.cms.gov/Research-Statistics-Data-and-Systems/Statistics-Trends-and-Reports/Beneficiary-Snapshot/Downloads/Bene_Snapshot.pdf)

## H Extended Results from the RL Analysis

### H.1 Policy Examples

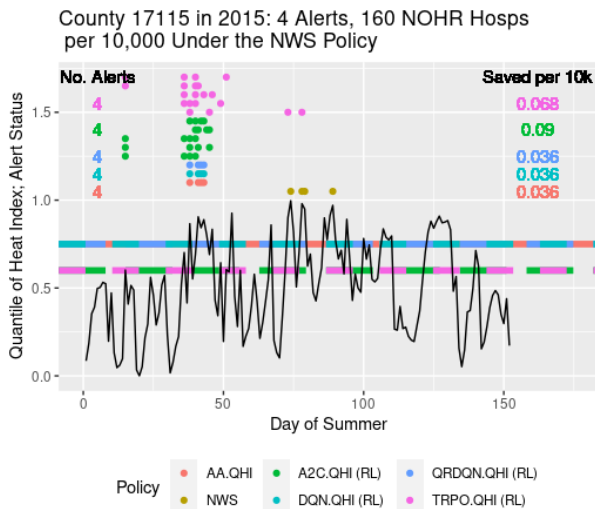


Figure S5: Example of a setting with relatively few heat alerts.

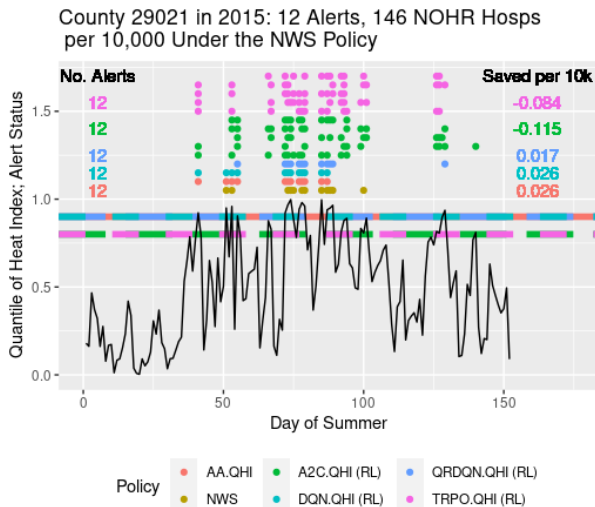


Figure S6: Example of a setting where implementing RL would not be beneficial relative to NWS or AA.QHI.

### H.2 Additional Discussion of Stochastic vs Deterministic Policies

Interpreting policies from the TRPO and A2C models deterministically fails because many of the policy functions' estimated probabilities for issuing an alert are below 0.5, so always taking the action with the larger probability dramatically reduces the number of alerts issued—in some counties to zero. Note that policies which do not use all the alerts

in their budget are penalized by the specification of our rewards model, resulting in DET.TRPO.QHI and DET.A2C.QHI no longer outperforming NWS with statistical significance across the 30 counties. Inclusion of future information mitigates this issue, but the results are not nearly as good as their stochastic counterparts.

Our big picture intuition for this result is that we are in a heavily data-constrained setting, which frustrates RL's ability to completely identify alert fatigue. The stochastic models address this by sampling alert days, inducing less alert streaks. Thought a bit unsatisfying, we believe this is an acceptable compromise given that, as mentioned in the main text, an online heat alert-RL system would likely utilize stochastic exploration anyway, to update itself over time.

### H.3 Additional Figures from the Post-hoc Contrastive Analysis

Figure S7 provides histograms of different policies' temporal characteristics, and figures S8, S9, and S10 illustrate the CART analysis.

Policy	Median Diff.	WMW	P-value	NOHR Hosps Saved vs NWS (vs Zero) Per Summer	
				Median / 10,000 Medicare	Approximate Total
*TOPK	0.022	406	0.0002	0.023 (1.96)	113 (9,603)
RANDOM	-0.015	177	0.88	-0.013 (1.98)	-64 (9,697)
BASIC.NWS	-0.286	30	1.0	-0.283 (1.45)	-1,388 (7,110)
AA.QHI	0.03	348	0.0025	0.029 (1.99)	143 (9,747)
DQN	-0.123	43	0.99995	-0.102 (1.83)	-502 (8,989)
QRDQN	-0.117	51	0.99991	-0.098 (1.85)	-480 (9,046)
TRPO	-0.065	97	0.99742	-0.063 (1.9)	-309 (9,321)
A2C	-0.063	100	0.99689	-0.062 (1.9)	-301 (9,317)
DQN.QHI	0.03	370	0.00242	0.029 (1.99)	142 (9,746)
QRDQN.QHI	0.035	344	0.01121	0.031 (1.99)	153 (9,767)
TRPO.QHI	0.038	338	0.0154	0.038 (2.02)	185 (9,897)
A2C.QHI	<b>0.042</b>	344	0.01121	0.045 (2.02)	222 (9,902)
DQN.F	-0.417	40	0.99996	-0.401 (0.49)	-1,966 (2,408)
QRDQN.F	-0.42	48	0.99993	-0.42 (0.47)	-2,059 (2,322)
TRPO.F	-0.062	103	0.99625	-0.061 (1.9)	-297 (9,322)
A2C.F	-0.063	101	0.99669	-0.062 (1.9)	-302 (9,304)
DQN.QHI.F	-1.895	1	1	-1.901 (0)	-9,317 (0)
QRDQN.QHI.F	0.014	238	0.45904	0.012 (1.61)	61 (7,876)
TRPO.QHI.F	<b>0.046</b>	345	0.01062	0.048 (2.02)	236 (9,886)
A2C.QHI.F	0.036	343	0.01183	0.038 (2.02)	187 (9,915)
DET.TRPO.QHI	-0.662	57	0.99985	-0.579 (0)	-2,835 (2)
DET.A2C.QHI	-0.886	90	0.99837	-0.794 (0.16)	-3,888 (807)
DET.TRPO.QHI.F	<b>0.032</b>	271	0.21723	0.034 (1.83)	168 (8,948)
DET.A2C.QHI.F	0.02	287	0.13335	0.021 (2.01)	104 (9,836)

Table S5: Extension of Table 1 to illustrate the comparisons in terms of absolute hospitalizations. Comparison between the average return of each counterfactual policy and that of the NWS policy on the evaluation years, summarized across counties (e.g. “Median Diff.” is the median difference in average return). The last two columns also provide a comparison to the counterfactual with zero heat alerts issued. WMW is the Wilcoxon-Mann-Whitney statistic (higher is better); its associated p-value is also included. The first policy, marked by \*, requires oracle knowledge of the future weather. The approximate total number of hospitalizations is based on 49 million Medicare enrollees in 2011 (CMS 2011).

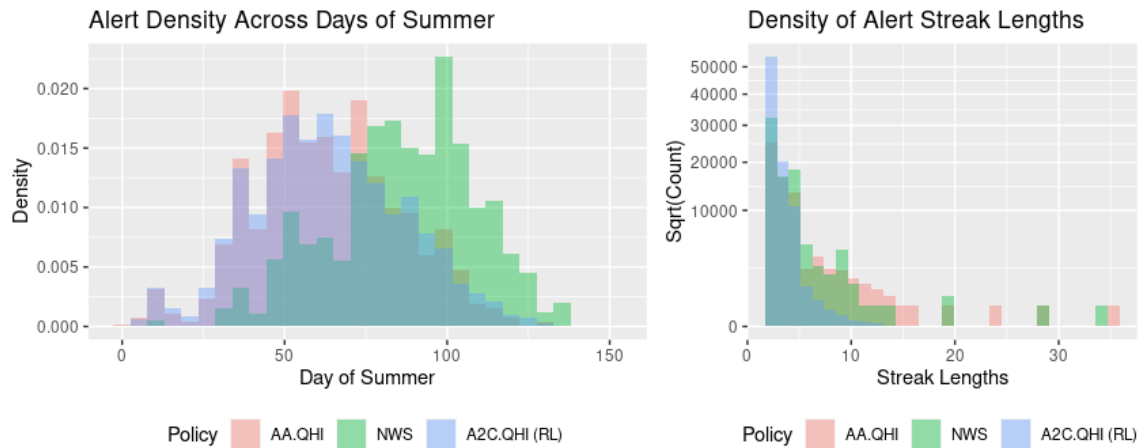


Figure S7: Distributions of heat alert characteristics under different policies, over the evaluation years.

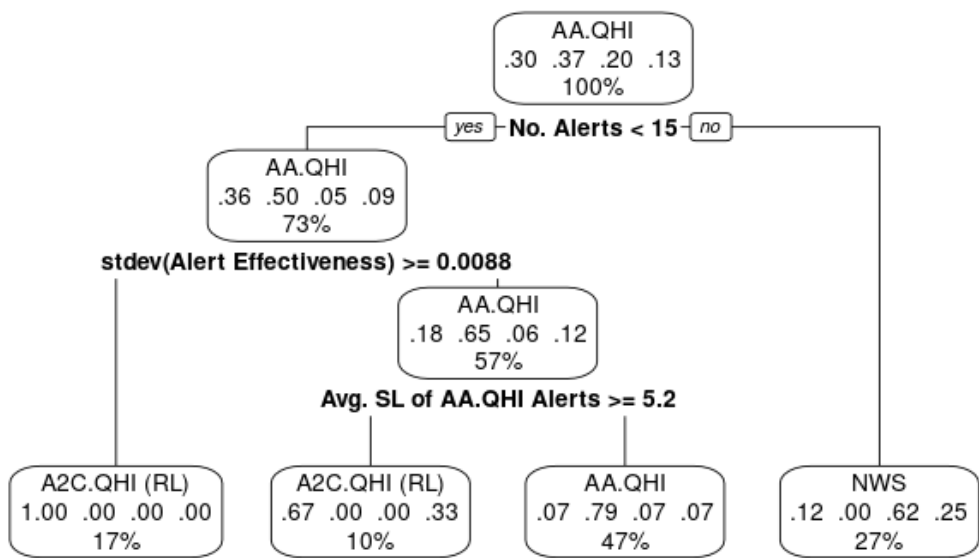
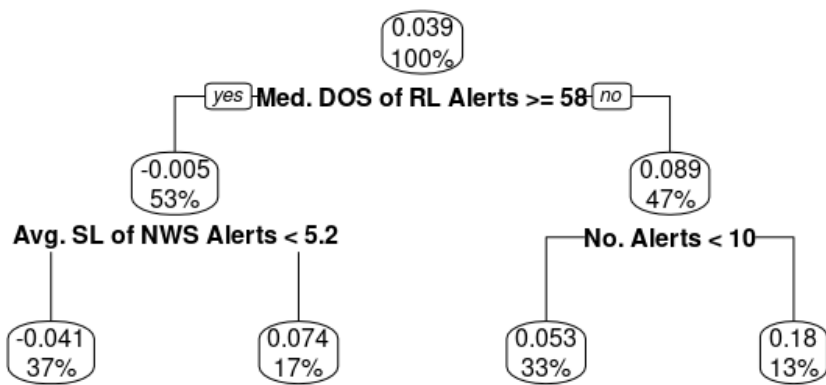
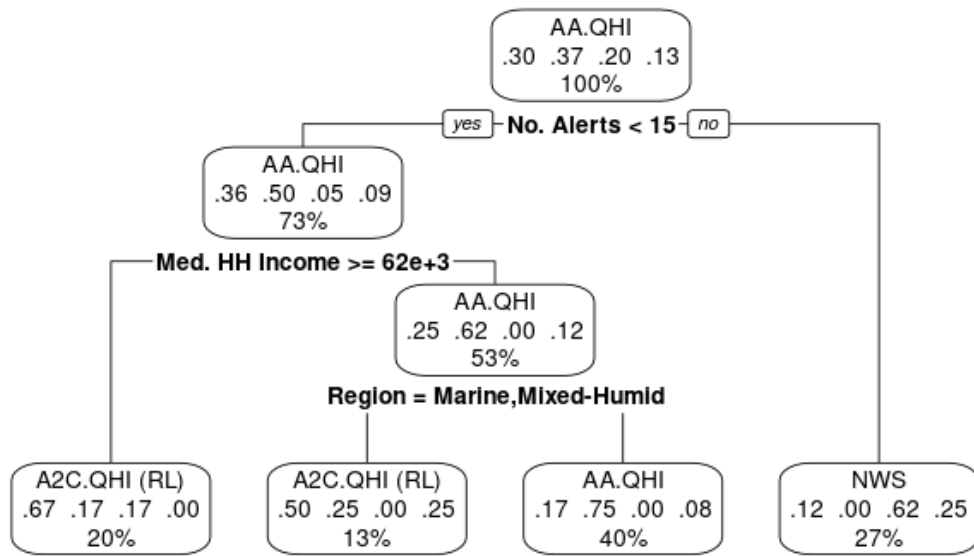


Figure S8: Polytomous classification tree comparing A2C.QHI, AA.QHI, NWS, and TRPO.QHI across the 30 counties. Within each node, the policy at the top is that associated with the highest probability of performing best. The four probabilities beneath correspond to the four policies in alphabetical order, as written above. (Note that the two RL policies tend to be more similar to one another, as do the AA.QHI and NWS policies, so the distribution of probabilities is important to consider in addition to the overall classification of each node.) The percentage at the bottom is the fraction of counties represented by that node. “No. Alerts” is the average number of heat alerts per warm season during the evaluation years, “Alert Effectiveness” is the  $\tau$  estimated by our rewards model, and SL is the streak length.



## Appendix References

Bell, A.; and Jones, K. 2015. Explaining fixed effects: Random effects modeling of time-series cross-sectional and panel data. *Political Science Research and Methods*, 3(1): 133–153.

CMS. 2011. 2011 CMS Statistics. Technical report, U.S. Department of Health and Human Services.

Dahl, K.; Licker, R.; Abatzoglou, J. T.; and Declet-Barreto, J. 2019. Increased frequency of and population exposure to extreme heat index days in the United States during the 21st century. *Environmental Research Communications*, 1(7): 075002.

Eimer, T.; Benjamins, C.; and Lindauer, M. 2022. Hyperparameters in Contextual RL are Highly Situational. ArXiv:2212.10876 [cs].

Gelman, A. 2006. Prior distributions for variance parameters in hierarchical models (Comment on Article by Browne and Draper). *Bayesian Analysis*, 1(3): 515–534.

Han, D.; Mulyana, B.; Stankovic, V.; and Cheng, S. 2023. A Survey on Deep Reinforcement Learning Algorithms for Robotic Manipulation. *Sensors (Basel, Switzerland)*, 23(7): 3762.

Metzger, K. B.; Ito, K.; and Matte, T. D. 2010. Summer Heat and Mortality in New York City: How Hot Is Too Hot? *Environmental Health Perspectives*, 118(1): 80–86.

Nobre, W. S.; Schmidt, A. M.; and Pereira, J. B. 2021. On the effects of spatial confounding in hierarchical models. *International Statistical Review*, 89(2): 302–322.

Tec, M.; Trisovic, A.; Audirac, M.; Woodward, S.; Hu, J. K.; Khoshnevis, N.; and Dominici, F. 2024. SpaCE: The Spatial Con founding Environment. In *International Conference in Learning Representations (ICLR)*.

The Boards of Trustees of the Federal Hospital Insurance and Federal Supplementary Medical Insurance Trust Funds. 2023. 2023 Annual Report. Technical report, Centers for Medicare & Medicaid Services.

The Commonwealth Fund. 2021. Medicare Advantage vs. Traditional Medicare: How Do Beneficiaries' Characteristics and Experiences Differ? <https://www.commonwealthfund.org/publications/issue-briefs/2021/oct/medicare-advantage-vs-traditional-medicare-beneficiaries-differ>. Accessed: 2024-01-01.

Tomczak, M.; Swaroop, S.; and Turner, R. 2020. Efficient Low Rank Gaussian Variational Inference for Neural Networks. In *Advances in Neural Information Processing Systems*, volume 33, 4610–4622. Curran Associates, Inc.

Wang, Y.; Miller, A. C.; and Blei, D. M. 2019. Comment: Variational Autoencoders as Empirical Bayes. *Statistical Science*, 34(2): 229–233.